Eur. J. Mineral.
2008, **20**, 73–94
Published online January 2008

Environmental factors controlling the precipitation of Cu-bearing hydrotalcite-like compounds from mine waters. The case of the "*Eve verda*" spring (Aosta Valley, Italy)

SIMONE TUMIATI[1,*,**], GASTON GODARD[2], NORBERTO MASCIOCCHI[1], SILVANA MARTIN[1] and DAMIANO MONTICELLI[1]

[1] Dipartimento di Scienze Chimiche e Ambientali, Università degli Studi dell'Insubria, via Valleggio 11, 22100 Como, Italy
*Corresponding author, e-mail: simone.tumiati@unimi.it
**Now at: Dipartimento di Scienze della Terra "Ardito Desio", Università degli Studi di Milano, via Botticelli 23, 20133 Milano, Italy
[2] Équipe Géobiosphère actuelle et primitive, Institut de Physique du Globe de Paris et Université Paris-Diderot, CNRS, 2 place Jussieu, 75005 Paris, France

Abstract: In the Cu–Fe-sulphide mining district of Servette-Chuc (Saint-Marcel, Aosta Valley, Italy), a streambed called *Eve Verda* and covered with a colloidal blue-green precipitate has been known since the 18th century. X-ray and chemical analyses reveal that the precipitate is a mixture of a nanocrystalline Cu–Al-sulphate hydrotalcite-like compound close to hydrowoodwardite ($Cu_{1-x}Al_x[SO_4]_{x/2}[OH]_2 \cdot mH_2O$) (49 ± 10 vol.%), and amorphous Al and Si oxyhydroxides. The Al/(Al + Cu) ratio of hydrowoodwardite (*i.e.*, x) ranges between 0.10 and 0.30 with a mean value of 0.17 ± 0.04. The average formula may be expressed as follows: $Cu_{0.81}Zn_{0.02}Al_{0.17}(SO_4)_{0.08}(OH)_2 \cdot 1.10\ H_2O$.

In order to construct phase diagrams, we estimated the thermodynamic properties of the hydrowoodwardite solid solution starting from calorimetric measurements available in the literature, *i.e.*, those for Mg, Co, Ni and Zn hydrotalcites. At least for $x < 0.35$, hydrowoodwardite may be treated either as an ideal or as a non-ideal solid solution between the two end-members $Cu(OH)_2$ (spertiniite) and $Al(SO_4)_{0.5}(OH)_2$ (aluminite). For $x = 1/3$ (*i.e.*, woodwardite *sensu stricto* following IMA nomenclature) and $m = 0$, the ideal solid solution model provided a Gibbs free energy of formation (ΔG_f^0) of –684.4 kJ/mol and an enthalpy of formation (ΔH_f^0) of –795.0 kJ/mol, while the non-ideal solution model yielded $\Delta G_f^0 = -658.6$ kJ/mol and $\Delta H_f^0 = -767.5$ kJ/mol. The estimated data agree well with the solubility measurements reported for hydrotalcites.

Since hydrowoodwardite precipitates where mineralised, acidic waters from an ephemeral stream are mixing with alkaline, diluted waters of a perennial spring, we calculated pH–X_w pseudosections (*i.e.*, isochemical phase diagrams), where X_w is the molar proportion of the two mixing waters. The thermodynamic modelling indicates that the formation of hydrowoodwardite is related to a geochemical barrier represented by the perennial spring waters. It also demonstrates that the composition of hydrowoodwardite (*i.e.*, x) is mainly a function of pH, while the modal composition of the precipitate depends instead on X_w. This explains the variations observed in the precipitate composition at *Eve Verda*.

Key-words: layered double hydroxides, hydrotalcite, copper, mine water, secondary phase, thermodynamic modelling.

Riassunto: Nel distretto minerario di Servette-Chuc (valle di Saint-Marcel) nella Valle d'Aosta, dove era coltivata in passato una mineralizzazione a solfuri di rame e ferro, è presente un piccolo corso d'acqua, il cui letto appare ricoperto da un precipitato colloidale blu-verde. Questo torrente, chiamato nei diversi idiomi Acqua Verde, Eve Verda o *Eaux vertes*, venne descritto per la prima volta da vice balivo Joseph Rambert nel 1749. Circa cinquanta anni dopo, Horace-Bénedict de Saussure, il grande precursore della geologia alpina, fornì la prima analisi chimica del precipitato nel suo *Voyages dans les Alpes* (1796).

In questo articolo presentiamo nuove approfondite analisi del precipitato blu-verde per determinarne la natura e la genesi. Le analisi chimiche e lo studio ai raggi X mostrano che il precipitato è una mistura d'idrowoodwardite nanocristallina (responsabile della colorazione blu-verde) e ossidrossidi d'alluminio e silicio amorfi (responsabili della colorazione biancastra). Per quanto riguarda la genesi, dimostriamo, grazie alla modellazione termodinamica, che l'idrowoodwardite si forma come conseguenza del disgelo estivo, quando le acque di drenaggio della soprastante miniera di Servette, acide e ricche in sali disciolti, si uniscono in piccola parte (circa il 6,5 %) alle acque alcaline e scarsamente mineralizzate di una sorgente perenne. Fungendo da barriera geochimica, le acque alcaline causano la precipitazione dell'alluminio e del rame in soluzione sotto forma d'idrowoodwardite,

DOI: 10.1127/0935-1221/2008/0020-1782
0935-1221/08/0020-1782 $ 9.90

minerale dal colore blu-verde. Durante l'inverno, il gelo impedisce alle acque acide di miniera di scorrere a valle e viene dunque a mancare l'apporto in sali necessari per stabilizzare l'idrowoodwardite. Di conseguenza, il precipitato invernale risulta arricchito in idrossido d'alluminio e assume una colorazione tendente al bianco.

Considerato da Rambert nel 1749 come un disastro ecologico, *Eve Verda* è invece un fenomeno eccezionale e spettacolare, che deve essere visto come una bella curiosità del patrimonio naturalistico della Valle d'Aosta.

1. Introduction

Mineral encrustations and precipitates ranging in colour from blue to green are commonly found as supergenic products after primary Cu and Cu–Fe sulphides, which are unstable under wet oxidising conditions (*e.g.*, Faure, 1998). Typically, Cu-rich secondary minerals have been ascribed in the scientific literature to carbonates, sulphates, silicates and, less commonly, oxides and hydroxides. However, recent studies emphasised the widespread occurrence and the high stability in the environment of more complex mineral species, such as hydrotalcites, minerals with the general formula $M^{2+}_{1-x}M^{3+}_{x}(A^{n-})_{x/n}(OH)_2 \cdot mH_2O$ (*e.g.*, Gade *et al.*, 2001; Allada *et al.*, 2002; Johnson & Glasser, 2003; Schubert *et al.*, 2005; Peltier *et al.*, 2006). Although Cu-bearing hydrotalcites have been mentioned in secondary ore parageneses (*e.g.*, Meixner, 1940; Nickel, 1976; Raade *et al.*, 1985; Livingstone, 1990; Witzke, 1999), comprehensive studies that throw light on the genesis of these minerals in the superficial environment are missing, probably because of the lack of thermodynamic data for such phases. Since hydrotalcites have been proved to control the transition-metal solubility in waters (Allada *et al.*, 2002; Peltier *et al.*, 2006), such studies would be very interesting not only from an academic perspective, but also for environmental purposes.

We chose for our study a classic site, known among scientists since the 18th century. It involves a spring and its related stream located in the Saint-Marcel valley, near Aosta (north-western Italy). The peculiarity of this stream is the abundance of a blue-green precipitate that covers the streambed. Our analyses revealed that the precipitate can be considered a nanocrystalline mixture of Al and/or Si oxyhydroxides with Cu-rich hydrowoodwardite, *i.e.*, $Cu_{1-x}Al_x(OH)_2(SO_4)_{x/2} \cdot mH_2O$ with $x \approx 0.17$ and $m \approx 1.10$.

In the following paragraphs, after a presentation of the occurrence (Sect. 2), we provide a mineralogical characterisation of the precipitate (Sect. 3) and then propose a model, supported by thermodynamics, for the genesis of this deposit (Sect. 4). In Section 5, we present an overview of hydrowoodwardite in the environment and discuss the contribution of our study to this question.

2. Occurrence of *Eve Verda*

The *Eve verda* or *Acqua verde* ("green waters") spring is located in the Cu–Fe mining district of Chuc–Servette (UTM coordinates: 379250 E, 5062250 N, Zone 32; 1370 m of altitude), near Saint-Marcel in the Aosta Valley (Italy) (Fig. 1). The peculiarity of this spring and the fed stream is the abundance of a Cu-rich blue-green deposit that covers the streambed over a length of about 150 m (Fig. 2), an amazing phenomenon that has fascinated scientists since the 18th century.

2.1. History

In September 1749, the vice-bailiff Joseph Rambert described a streambed covered with an unusual green substance near Saint-Marcel in the Duchy of Aosta. He was entrusted with an inquiry after the complaints of inhabitants of Saint-Marcel about the operators of a copper mine who were accused of polluting the waters and air of the area, and being responsible for bad crops and vintages. In his report, published by Nicco (1988), Rambert recounted that the water of the stream was greenish, had a bad smell and deposited a green "sediment". A few citizens of Saint-Marcel testified that the phenomenon had arisen after the digging of mine galleries from which the foul water flowed. Hence, Charles-Emmanuel III, King of Sardinia-Piedmont, prohibited ore treatment during the period from May to August. The vineyards recovered, it seems, but the green matter continued to precipitate and is still precipitating two and a half centuries later. The stream has been called *Eaux vertes* (in French), *Acqua verde* (in Italian) or *Eve verda* (in dialect), which mean "green waters".

Saint-Martin de La Motte, a member of the *Académie royale des Sciences* of the Sardinia-Piedmont Kingdom, made a series of analyses and observations on the water and its green deposit in which he detected copper (La Motte, 1784–85). In his *Voyages dans les Alpes*, Horace-Bénedict de Saussure (1796), the great precursor of Alpine geology, also described *Eve verda*, which he visited on the 20th of August 1792. He performed the first chemical analysis of the turquoise-green gel that covers the streambed obtaining: copper (19 wt.%), iron oxide (4.25 %), "carbonic acid" (H_2CO_3: 9 %), "clay" (2.75 %), "*calce*" (CaO: 1 %), silica (SiO_2: 33 %), water and other volatile components (31 %). The French mineralogist Jean-Pierre Bertrand de Lom (1844) gave a further description of this material, which he attributed to a new hydrosilicate of Cu and Al that he proposed to call "*chalcogélide*". The mineralogist Achille Delesse (1846) tried to characterise the substance collected by Bertrand de Lom, but concluded, on the basis of its instability and variations in composition, that it was likely a hydrated mixture of CuO, SiO_2 and Al_2O_3, rather than a new mineral species.

In 1903, Besse & Vaccari noticed that the green matter precipitates at the confluence of two streams, whereas Prosio (1903) discerned seasonal variations in it, with compositions ranging from a green Cu-rich component towards a white Cu-poor end-member. While making a survey of similar deposits in the Aosta Valley, Éphise Noussan (1972) described a comparable occurrence near Valmeriana.

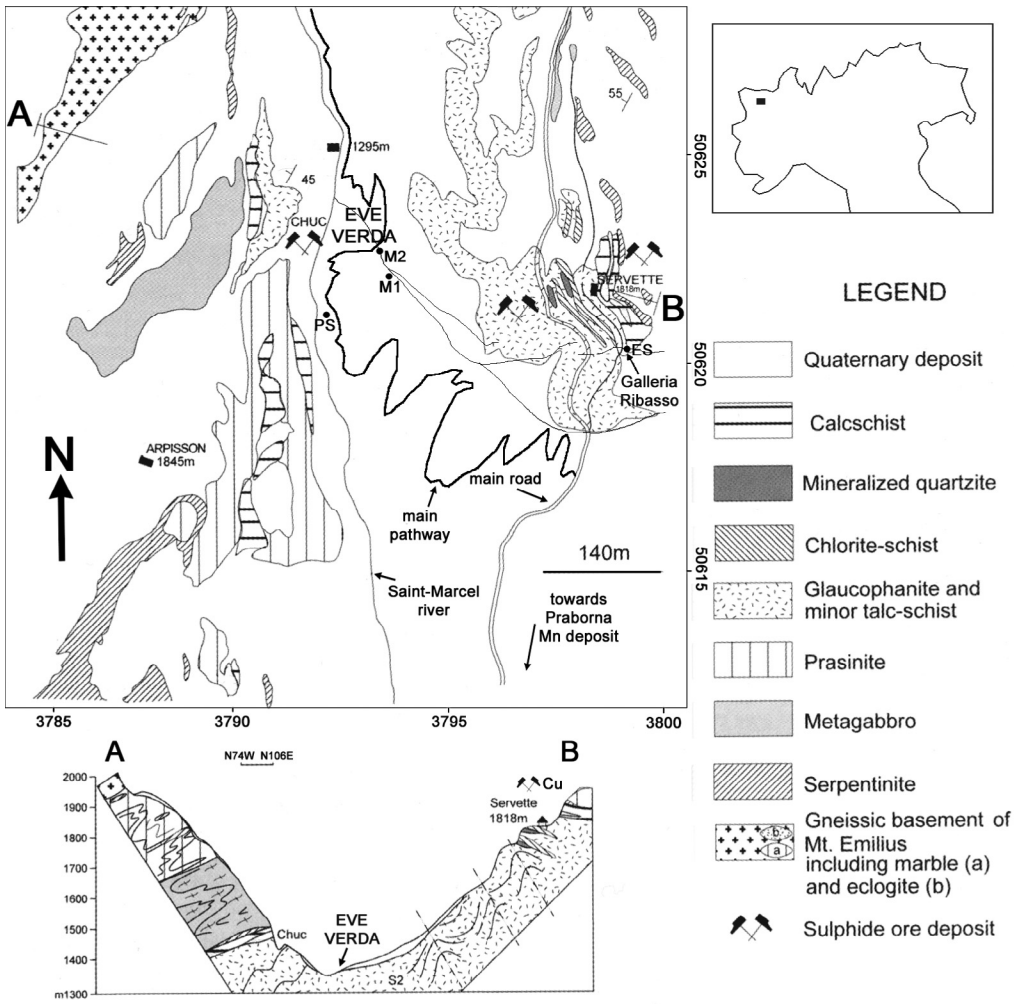

Fig. 1. Geological map and section of the Servette-Chuc area with the location of the *Eve verda* and *Galleria Ribasso* springs (see Table 1), modified after Martin *et al*. (2004). Displayed coordinates are UTM × 10^{-2}, zone 32.

In October 2000, the deposit completely disappeared during a catastrophic flow. However, it progressively reappeared during the following months, so the site could be visited during the 32nd International Geological Congress of Florence (Martin *et al.*, 2004).

2.2. Environmental setting

The Servette-Chuc mining district belongs to the Zermatt-Saas meta-ophiolite unit, which here consists of interlayered chloriteschists, talcschists, glaucophanite, quartzite, slices of eclogite-facies metagabbro and serpentinite (Fig. 1; Martin *et al.*, 2004). The sulphide deposit is concentrated in ENE-dipping layers of 3–4 m in thickness, but it is also disseminated throughout in the surrounding rocks (Cesti, 1978; Martin *et al.*, 2004). The ore assemblage consists of pyrite and chalcopyrite, with other minor sulphides such as sphalerite, bornite, digenite, pyrrhotite, marcasite and mackinawite (Martin *et al.*, 2004, and references therein). The walls of the abandoned galleries of the mine are covered with encrustations, in which the presence of sulphates, Cu-bearing silicates and carbonates has been reported. Pelloux (1908), Scaini (1971) and Cesti (1978) mentioned gypsum, epsomite ($MgSO_4 \cdot nH_2O$), chalcanthite ($CuSO_4 \cdot 5H_2O$), copiapite ($Fe^{2+}\ Fe_4^{3+}\ [SO_4]_6\ [OH]_2 \cdot n\ H_2O$), slavikite ($NaMg_2Fe_5^{3+}[SO_4]_7[OH]_6 \cdot 33H_2O$), chrysocolla and malachite.

A few hundred metres below Chuc, the main pathway crosses a small rocky stream (see *Eve verda* in Fig. 1). From a certain point located a few metres uphill, its streambed rocks and pebbles are covered with a blue-green precipitate (Fig. 2). There, waters of a perennial spring (PS in Fig. 1), which pours out from a slope and/or landslide debris, get mixed (M1, M2 in Fig. 1) with those of an ephemeral stream, characterised by a yellow-coloured bed rich in iron hydroxides. These last waters, which flow only during summer, come from *Galleria Ribasso*, an upper drainage gallery of the Servette mine situated at an altitude of 1789 m (ES in Fig. 1).

The ephemeral spring waters are characterised by an acidic pH of about 3 (ES in Table 1). On the other hand, the waters of the perennial spring (PS in Table 1) display an alkaline pH of 8.14. The two waters also have different

Fig. 2. The *Eve verda* stream in the Spring of 2003.

dissolved-salt contents. For example, the sulphate concentration is 1007 mg/L and 58.43 mg/L, respectively in the ES and PS waters. Of great importance for our study is the content of dissolved Cu, which ranges from 34.14 mg/L (ES) to 1.22×10^{-3} mg/L (PS), and Al, from 23.29 mg/L (ES) to 4.36×10^{-3} mg/L (PS). Looking at these data, we can infer that the components of the ES waters are controlled by the weathering of the Servette-Chuc Cu–Fe sulphide ore, which accounts for the SO_4^{2-}, Cu^{2+} and H^+ water enrichment. On the other hand, the PS waters do not interact with the Cu mineralization.

3. Characterisation of the precipitate

3.1. Crystallography

We carried out X-ray powder diffraction (XRPD) analyses of 8 different samples of some blue-green material collected (i) along the *Eve verda* stream bed (springs M1, M2 in Fig. 1; samples 1a, 1b, 4, 5 in Table 2) and (ii) on the walls of the upper *Galleria Ribasso* (ES in Fig. 1; samples 2, 3, 6a, 6b in Table 2). Details concerning the analytical conditions can be found in the Appendix.

3.1.1. X-ray powder diffraction analysis

The diffraction patterns display both broad and sharp peaks, suggesting the occurrence of phases characterised by different degrees of crystallinity (Fig. 3). In the wall encrustations of *Galleria Ribasso*, among the crystalline phases, we found the hydrated Cu-hydroxycarbonate malachite in 4 samples, and the hydrated Cu-sulphate posnjakite in 2 samples (Table 2; Fig. 3). In the samples coming from *Eve verda*, we found detrital minerals, such as chlorite (in 2 samples), quartz (in 2 samples) and muscovite (in one sample).

In all samples from both sites, the systematic occurrence of broad peaks in similar angular positions suggests the presence of a shared phase that is not completely amorphous. The percentage of this phase compared to the other minerals is variable, being minimal in dark-green hard encrustations (see the malachite-rich samples 6a and 6b) and maximal in light blue-green soft colloidal deposits (samples 1a, 1b, 3). The mean, maximum and minimum *d*-spacings obtained from the diffraction patterns are shown in Table 2. In all samples, except sample 5, the maximum intensity is displayed by the broad peak characterised by *d*-spacings ranging from 7.04 to 11.98 Å. Among these low-2θ° peaks, the lower *d*-spacings are displayed by the phase contained in sample 3 (d = 7.71 +1.11/–0.67 Å), while the higher *d*-spacings are shown by the phase contained in sample 4 (d = 11.20 +0.78/–0.56 Å). Other important peaks ranging from 2.40 to 2.68 Å display a minor shift among samples. We noted that such peaks become enhanced in dried and aged specimens characterised by a clear loss of crystallinity. In sample 5, a broad peak at about 2.60 Å is the only one recognisable (Table 2), suggesting that this material was already nearly amorphous *in situ*. Peaks that display a large shift among samples and weak intensity are situated in a *d* range from 3.41 to 4.44 Å.

Comparing the diffraction pattern of the observed phase with those reported in the database of the International Centre of Diffraction Data (ICDD), we find analogies with minerals belonging to the hydrotalcite group. Hydrotalcites (HTlc) are minerals that have recently attracted the attention of chemists because of their applications as catalysts and anion exchangers (see for example Allada *et al.*, 2002). These minerals have the general formula $M^{2+}_{1-x}M^{3+}_{x}(OH)_2[A^{n-}]_{x/n} \cdot mH_2O$. Their structure was first elucidated in the FeO–MgO–Al_2O_3–H_2O–CO_2 system by Allmann & Lohse (1966) and Allmann (1968). It is composed of positively charged brucite-type metal-hydroxide layers intercalated with anions $[A^{n-}]$ and water molecules (Fig. 4). For this reason, these minerals are also often called *layered double hydroxides* (LDH; see for example Peltier *et al.*, 2006). The structure accommodates a number of cations (for example, Mg, Co, Ni, Zn among bivalent, and Al, Fe, Cr among trivalent cations), interlayer anions (CO_3, NO_3, SO_4, Cl) and variable amounts of water (Allada *et al.*, 2002) (see Table 3 concerning Al-hydrotalcites).

3.1.2. Some crystallographic remarks

For the reasons outlined below, we prefer to discuss the X-ray diffraction traces obtained in terms of *d*-spacings (directly accessible from the scattering angles of the broad

Table 1. Measured water compositions in the *Eve verda* area. After Terrana (2006), modified.

	ephemeral spring		perennial spring		mixed waters			
	ES		PS		M1		M2	
pH	2.98		8.14		7.39		7.55	
T °C	4.1		6.1		5.8		7.2	
X_w	1.000		0.000		0.058		0.058	
precipitate	yellow		none		blue-green (sample 1)		blue-green	
	ppm	mol/L	ppm	mol/L	ppm	mol/L	ppm	mol/L
CO_2	69.91	1.59E-03	<dl	-	<dl	-	<dl	-
HCO_3^-	<dl	-	164.94	2.70E-03	101.41	1.66E-03	98.71	1.62E-03
Cl	<dl	-	0.36	1.02E-05	0.91	2.57E-05	2.2	6.21E-05
SO_4^{2-}	1007.18	1.05E-02	58.43	6.08E-04	92.02	9.58E-04	92.75	9.66E-04
Ca	89.1	2.22E-03	44.01	1.10E-03	42.62	1.06E-03	40.39	1.01E-03
Mg	51.4	2.11E-03	4.68	1.93E-04	5.99	2.46E-04	4.99	2.05E-04
SiO_2	11.27	1.88E-04	4.77[a]	7.94E-05	3.3	5.49E-05	3.2	5.33E-05
Cu[b]	34.14	5.37E-04	1.22E-03	1.92E-08	4.00E-01	6.29E-06	2.88E-01	4.52E-06
Fe[b]	84.43	1.51E-03	nd	-	9.80E-03	1.75E-07	2.11E-01	3.78E-06
Al[b]	23.29	8.63E-04	4.36E-03	1.62E-07	4.01E-02	1.49E-06	6.07E-02	2.25E-06
Cr[b]	6.00E-02	1.15E-06	8.40E-04	1.62E-08	4.10E-04	7.89E-09	5.50E-04	1.06E-08
Co[b]	1.90	3.22E-05	3.20E-04	5.43E-09	6.48E-02	1.10E-06	6.33E-02	1.07E-06
Zn[b]	7.10	1.09E-04	2.38E-03	3.64E-08	2.10E-01	3.20E-06	1.76E-01	2.69E-06
Sr[b]	1.55E-01	1.77E-06	1.12E-01	1.28E-06	1.25E-01	1.42E-06	1.22E-01	1.39E-06
Pb[b]	7.20E-04	3.47E-09	<dl	-	3.00E-05	1.45E-10	4.00E-05	1.93E-10
U[b]	1.67E-03	7.02E-09	<dl	-	2.00E-05	8.40E-11	2.00E-05	8.40E-11

<dl = below detection limit.
nd = not determined.
a = estimated from Eq. (1) (Sect. 4.2.1) (this study).
b = analysed by ICP-MS.
X_w = ES/PS ratio calculated by mass balance (this study).

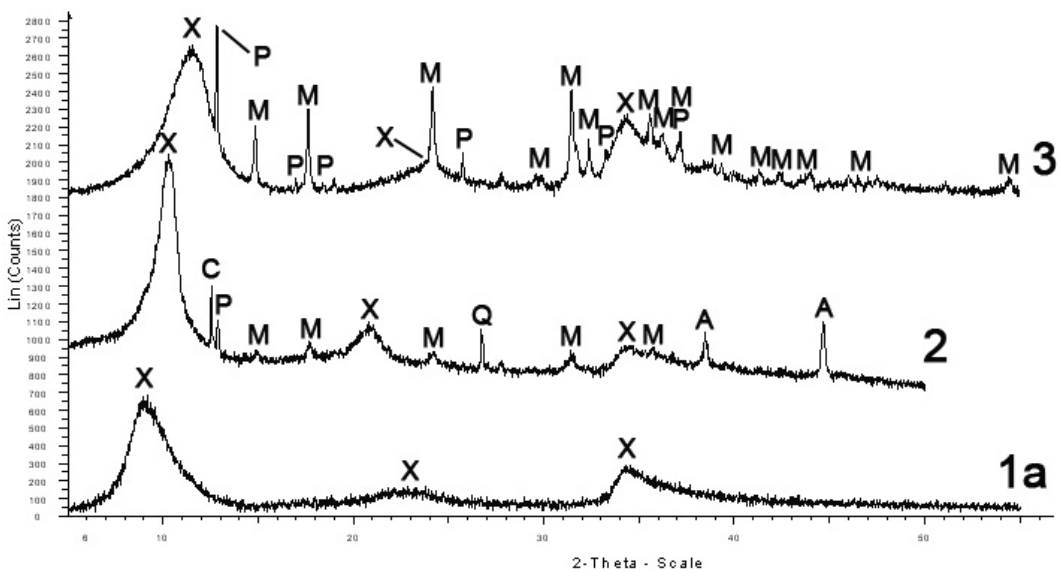

Fig. 3. X-ray diffraction patterns of samples 1a (from *Eve verda*), 2 and 3 (from *Galleria Ribasso*). The attribution of peaks to different species was carried out by matching with the ICDD database [P: posnjakite; M: malachite; Q: quartz; C: chlorite; A: aluminium (sample holder)]. "X" refers to the nanocrystalline hydrotalcite-like compound.

Table 2. X-ray diffraction data for the blue-green precipitate.

Sample	Origin	Aspect	Identified crystalline phases	*d*-spacings of the hydrotalcite-like phase (Å)			
				I	d_{mean}	d_{max}	d_{min}
1a	Eve verda; riverbed stone	light blue-green flakes	-	s	9.82	10.87	8.50
				w	3.90	4.21	3.64
				m	2.61	2.66	2.46
1b	Eve verda; riverbed stone	light blue-green flakes	-	s	10.21	8.85	7.35
				w	3.87	4.18	3.48
				m	2.59	2.66	2.43
				w	1.53	1.55	1.48
2	Galleria Ribasso; wall encrustation	light green crust	chlorite; quartz; posnjakite; malachite	s	8.62	9.25	8.21
				m	4.24	4.44	4.13
				mw	2.60	2.66	2.43
3	Galleria Ribasso; wall encrustation	light blue-green gel	posnjakite; malachite	s	7.71	8.82	7.04
				w	3.81	4.06	3.41
				m	2.61	2.68	2.41
4	Eve verda; filtered from waters	light blue-green	chlorite; muscovite; quartz	s	11.20	11.98	10.64
5	Eve verda; riverbed stone	light-green gel	-	s	2.60	2.68	2.40
6a	Galleria Ribasso; wall encrustation	emerald-green crust	malachite	s	8.95	10.28	8.37
6b	Galleria Ribasso; wall encrustation	emerald-green crust	malachite	s	8.97	9.83	8.69

"d_{max}" and "d_{min}" correspond to the peak width at half height, while d_{mean} corresponds to the peak maximum. *I* represents the observed intensity of the peak: w = weak, m = medium, s = strong.

peak maxima) and not on the basis of Miller indices of less-than-ideal polycrystalline species. Since for such species with nanometric coherence lengths the standard crystallographic (Bragg-like) approach fails, the structural features will be discussed in a semi-quantitative way, without reference to any average unit cell size and space group symmetry.

The above considerations stem from the observation of the layered nature of these species, closely resembling brucite or, more precisely, layered double hydroxides, in which the stacking periodicity and sequence can range from ideal ones (as in the 3*R* and 1*T* polytypes) to a broad distribution determined by the amount, frequency and ordering of the M^{2+} and M^{3+} and anion/water intercalation.

In some fortunate cases (see for example Bellotto *et al.*, 1996), these polycrystalline materials give XRPD patterns amenable to a conventional Rietveld-type structural refinement or suitable for a meaningful analysis by unconventional simulation programs (DiffaX software by Treacy *et al.*, 2005; *cf.* http://www.public.asu.edu/~mtreacy/DIFFaX.html; see also Treacy *et al.*, 1991). Alternatively, for inorganic materials showing turbostratic disorder in the stacking of layers, a rather complex and unconventional analysis can be adopted (Reynolds, 1989). More frequently, much less informative diffraction traces hamper the extraction of detailed structural and microstructural information. This is indeed the case for the many reports on the scattering properties of "woodwardite" and hydrowoodwardite (Nickel, 1976; Dinelli *et al.*, 1998; Witzke, 1999), honessite (Livingstone, 1990), glaucocerinite (Raade *et al.*, 1985) and carrboydite (Nickel & Clarke, 1976) samples, all characterised by the presence of only a few very broad peaks.

In several cases, (average) unit cells and space group symmetries were assigned on the basis of well crystallised isotype materials, without critically considering the real structural implications of the derived parameters. For example, unit cell parameters as large as 32.7 Å (in $R\bar{3}m$) have been proposed, in the presence of diffraction peaks of more than 2.0° (2θ) wide: if Scherrer's equation is employed, coherent domains of *less than 2 unit cells* would be computed; alternatively, if a simple strain model, accounting for a distribution of lattice parameters is employed (Langford, 1978), a $\Delta d/d$ value of about 11 % can be derived (thus implying, for a typical interlayer spacing of 10 Å, an approximate width of such distribution larger than 1 Å).

On the basis of these considerations, these nanocrystalline particles, in which significant disorder is present, hampering an average periodicity, can only be studied by total scattering analyses with the assessment of the local

Table 3. Composition and reported symmetry of different hydrotalcite-like compounds with the general formula: $M^{2+}_{1-x}Al_x(OH)_2[A^{n-}]_{x/n} \cdot mH_2O$.

	dominant M^{2+}	x = Al/(Al+M^{2+})	OH	A^{n-}	H_2O	reported symmetry
hydrotalcite	Mg	0.25	2.00	CO_3	0.50	$R\bar{3}m$
manasseite	Mg	0.25	2.00	CO_3	0.50	$P6_3/mmc$
quintinite	Mg	0.33	2.00	CO_3	0.67	$P6_322$. $P3_112$ or $P3_212$
caresite	Fe	0.33	2.00	CO_3	0.50	$P3_112$ or $P3_212$
charmarite	Mn	0.33	2.00	CO_3	0.50	$P6_322$, $P3112$
zaccagnaite	Zn	0.33	2.00	CO_3	0.50	$P6_3/mmc$
glaucocerinite	Zn	0.38	2.00	SO_4	1.13	Rhombohedral
zincowoodwardite	Zn	0.00–0.67	2.00	SO_4	0.59–0.96	$R\bar{3}m$ or $P\bar{3}$
zincaluminite	Zn	0.50	2.17	SO_4	0.42	Hexagonal
carbonate-cyanotrichite	Cu	0.33	2.00	CO_3, SO_4	0.33	Orthorhombic
woodwardite	Cu	0.33	2.00	SO_4	0.33–0.67	Rhombohedral
hydrowoodwardite	Cu	0.00–0.67	2.00	SO_4	>3x/2	$R\bar{3}m$
cyanotrichite	Cu	0.33	2.00	SO_4	0.33	Orthorhombic
chalcoalumite	Cu	0.80	2.40	SO_4	0.60	$P2_1$
spangolite	Cu	0.14	1.71	SO_4, Cl	0.43	$P31c$
takovite	Ni	0.25	2.00	CO_3	0.50	$R\bar{3}m$
nickelalumite	Ni	0.80	2.00	SO_4, NO_3	0.60	$P2_1$
carrbodyte	Ni	0.39	1.87	SO_4, CO_3	0.30	Hexagonal

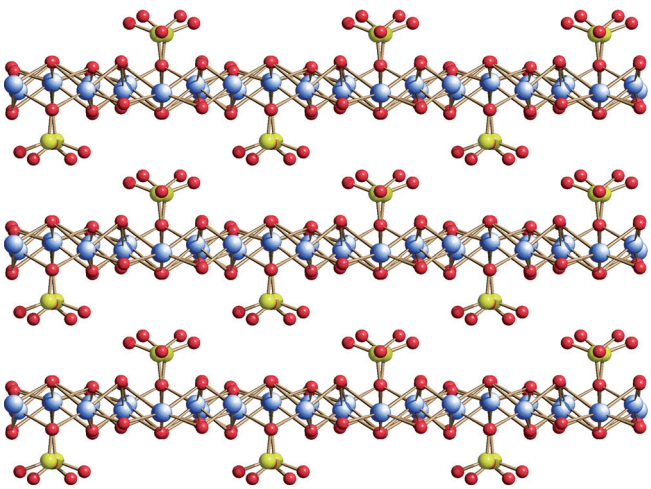

Fig. 4. Schematic drawing of an idealised (*i.e.*, periodic) $Cu_xAl_{1-x}(OH)_2(SO4)_{x/2}$ structure, based on brucitic layers. Drawing produced using the software SCHAKAL 99 (see Keller, 1980). Al, Cu: blue; S: yellow; O: red. The coordinates of most (but not all) atoms have been taken from the structure of $Zn_3(OH)_4(NO_3)_2$ (Louër *et al.*, 1973); sulphates have been added as tetrahedral ligands and the stacking sequence has been arbitrarily set at *ca.* 7 Å (that of the anhydrous hydroxy-nitrate structure). In woodwardite, Cu and Al ions (in blue) are disordered in the same crystallographic sites, and sulphates (in yellow) randomly occupy hydroxyl positions. In addition, water molecules are hosted among the layers, further increasing their separation to up to 10 Å. As reported in the text, the distance between these layers depends on the number, quantity and disposition of the spacers (sulphates and water molecules).

metal environments. In this case, pair distribution function (PDF) analysis or X-ray absorption methods are likely to afford a more detailed structural picture.

However, the diffraction traces collected during our study, as well as those reported in previous publications, coherently suggest the following crystallographic features:

a) the particles are built by the stacking of brucite-like layers, in which M^{2+} and M^{3+} ions are octahedrally coordinated (mostly) by hydroxide ions in the common μ_3-OH mode;
b) electroneutrality is maintained by the presence of di-anionic ligands, such as sulphates (or, in some cases, carbonates), sticking out on each side of the brucitic slabs. A simplified sketch of the local coordination environment of the metal ions in this kind of species is proposed in Fig. 4;
c) the separation between adjacent layers (discussed above in terms of the *d*-spacing of the most intense peak, 003 in the rhombohedral approximation) depends on the size and amount of these substituting ions, and is possibly assisted by the presence of interlayer crystallisation water;
d) each layer may, or may not, be perfectly planar, depending of the spatial distribution of the sulphate anions on each side;
e) a further disordering process, related to the presence of the Cu^{2+} ions, is the tendency of d^9 ions towards (static) Jahn-Teller distortion (which Al^{3+} would mitigate); that this effect can influence the local stereochemistry in copper containing layered double hydroxides is proved by the coherent periodic distortion in monoclinic Cu–Al-hydrotalcites (Yamaoka *et al.*, 1989) and by the extremely asymmetric coordination of Cu^{2+} in $Cu(OH)_2$, which does not conform to the archetypical CdI_2 structure, as many other $M^{2+}(OH)_2$ species do.

3.2. Chemical composition

In order to characterise the nanocrystalline hydrotalcite-like compound found in the precipitate, we analysed, with

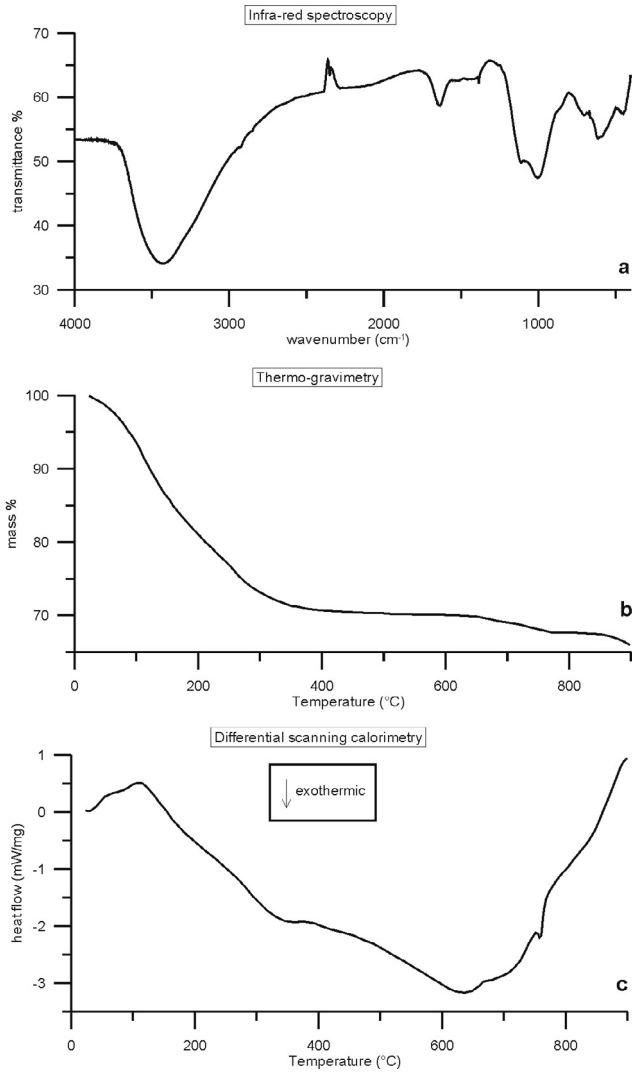

Fig. 5. a) Infra-red (IR) spectrum, b) thermo-gravimetric (TG) and c) differential-scanning-calorimetry (DSC) analyses of the blue-green precipitate (sample 1).

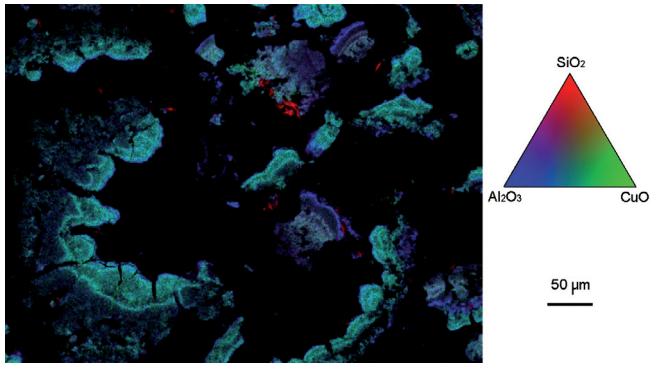

Fig. 6. EDX Si–Cu–Al image of the blue-green precipitate. Elemental images were acquired on sample 1 (*Eve verda*) with a scanning electron microscope (SEM) and combined in an RGB image (see Appendix for analytical conditions).

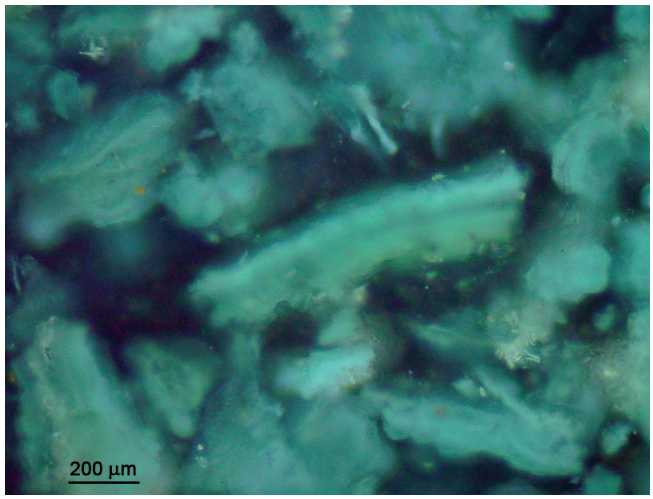

Fig. 7. Microphotographs of a polished section of the blue-green precipitate (sample 1) using an optical microscope (reflected crossed-polarised light).

different methods, sample 1 from *Eve verda*, the only one that does not show impurities of truly crystalline phases in X-ray diffraction patterns. Anion and cation contents were investigated by means of infra-red (IR) spectrometry, thermo-gravimetric (TG) analysis, differential scanning calorimetry (DSC), CHN elemental analysis and energy-dispersive X-ray analysis (EDX) mapping. Details concerning the analytical conditions can be found in the Appendix.

Bands of the IR spectrum (Fig. 5a) at 3423 and 1636 cm^{-1} are generally attributed to H_2O and OH vibrations (see for example Witzke & Raade, 2000) while bands below 1110 cm^{-1} are characteristic of the sulphate anion. Weaker bands occurring at 2928 and 2857 cm^{-1} and at about 1385 cm^{-1} are attributable to minor amounts of organic molecules and carbonates, respectively.

The TG curve (Fig. 5b) shows that dehydration of the blue-green matter starts at low temperature and continues up to 360 °C where the total mass loss accounts for 28.85 wt.%. This value is thought to be the total H_2O contained in the sample and has been confirmed by CHN analysis, which yielded an identical amount of 28.24 wt.% H_2O. CHN analysis also indicates a negligible N-content and 0.89 wt.% C, a large part of which should be due to organic impurities (see IR spectrum in Fig. 5a).

The DSC curve (Fig. 5c) shows an endothermic peak at 111.1 °C, most probably related to dehydration reactions, and an exothermic peak at 640 °C, where the loss of the sulphate groups begins and the whole framework collapses.

EDX elemental maps, collected on the dried sample 1 enclosed in epoxy resin, suggest that Cu, Al, Si and S are the most important elements contained in the precipitate. The distribution of the elements resembles stromatolite-like superposed films of different composition (Fig. 6). This heterogeneity is recognisable also with an optical microscope, as layers of a more-or-less intense blue coloration (Fig. 7). Obviously, deep-coloured layers are richer in Cu, while light-coloured ones are richer in Al and Si.

Table 4. Chemical and mineralogical composition of the precipitate (average of 210 electron-microprobe [EMP] analyses).

EMP analysis of the precipitate		
Oxides	wt.%	σ
MgO	0.05	0.04
Al_2O_3	11.97	4.42
SiO_2	7.86	3.88
SO_2	1.76	0.81
CaO	0.31	0.19
MnO	0.00	0.05
FeO	0.03	0.06
CoO	0.00	0.24
CuO	21.24	11.41
ZnO	0.57	0.29
Total	43.77	21.40
Normalisation to (100-wt.%H_2O-wt.%CO_2)		
MgO	0.08	0.07
Al_2O_3	19.51	7.21
SiO2	12.81	6.33
SO_2	2.86	1.32
CaO	0.51	0.31
MnO	0.00	0.08
FeO	0.05	0.10
CoO	0.00	0.39
CuO	34.64	18.61
ZnO	0.92	0.48
CO2*	0.40	0.25
H_2O**	28.24	-
Total	100.00	-

Hydrotalcite composition***		
Elements	moles	σ
$Cu(OH)_2$	0.81	0.04
$Zn(OH)_2$	0.02	0.01
$Al(OH)_2(SO_4)_{0.5}$	0.17	0.04
$m = H_2O$	1.10	-
Cu/(Zn+Cu)	0.97	0.01
x = Al/(Al+Cu+Zn)	0.17	0.04

Molar proportions in the precipitate		
Phases	mol.%	σ
Hydrotalcite	50.98	10.75
$Al(OH)_3$	27.89	9.06
SiO_2	20.27	4.13
$CaCO_3$	0.86	0.44

Modal proportions in the precipitate		
Phases	vol.%	σ
Hydrotalcite	48.98	10.33
$Al(OH)_3$	30.81	10.01
SiO_2	19.11	3.90
$CaCO_3$	1.10	0.56

* calculated on the basis of nCa = nCO2

** measured by CHN analysis

*** on the basis of the general formula

$M^{2+}_{1-x}M^{3+}_{x}(OH)_2(SO_4)_{x/2} \cdot mH_2O$

It appears that M^{2+}–Al hydrotalcites can be classified by individuating the main anion (SO_4, CO_3, NO_3, Cl) and the main M^{2+} cation (Cu, Zn, Ni, Mn, Fe), and by considering the M^{2+}/Al ratio. For this purpose, we performed point analyses on the same sample in order to achieve accurate chemical compositions. These were obtained with an electron microprobe (EMP), equipped with wavelength-dispersive spectrometers (WDS). Details concerning the analytical conditions can be found in the Appendix. Since the material is intrinsically porous, the analyses were partly mixed with the enclosing resin, yielding low totals. The average and standard deviation (σ) of 210 point analyses are shown in Table 4. Assuming that the complement to 100 wt.% of this average analysis corresponds to the enclosing resin and H_2O (+CO_2) contained in the material, we tried to extrapolate a resin-free analysis by normalising the average analysis to a total of (100-H_2O*-CO_2*) wt.%, where H_2O* is the value measured by CHN analysis and CO_2* is a value calculated considering $CaCO_3$ as the only source of both Ca and CO_2 (Table 4).

Low weight totals do not affect the calculation of molar proportions, as these are normalised. The hydrotalcite composition and the molar proportions of the phases that are thought to form the precipitate have been estimated by solving a set of C equations, where C (=6) is the number of independent components (*i.e.*, SiO_2, Al_2O_3, CuO, ZnO, SO_3, CaO), the minor components FeO, MgO, CoO and MnO having not be considered since their contents are negligible (Table 4). The C estimated independent variables are the Cu/(Zn+Cu) and Al/(Al+Cu+Zn) ratios in hydrotalcite, and the molar quantities of hydrotalcite, $Al(OH)_3$, SiO_2 and $CaCO_3$, which were normalised to 100 (Table 4). $Al(OH)_3$ and SiO_2 could exist in the precipitate as various Si and/or Al amorphous oxyhydroxides, such as gibbsite, silica, allophane (*i.e.*, an amorphous association of hydrated Si- and Al-oxides) and/or halloysite/kaolinite (*cf.* Certini *et al.*, 2006), which unfortunately cannot be identified because of the lack of characteristic X-ray diffraction peaks (*cf.* Sect. 3.1). The modal proportions of such phases cannot be estimated, as this would lead to an underdetermined set of equations.

Hydrotalcite occurs as 51 ± 11 mol.% of the total. The remainder is constituted almost entirely of $Al(OH)_3$ and, to a lesser extent, SiO_2. $CaCO_3$ only occurs in trace amounts (0.86 ± 0.44 mol.%). We notice that the hydrotalcite composition (Table 4) is compatible with that of hydrowoodwardite $(Cu,Zn)_{1-x}Al_x(SO_4^{2-})_{x/2}(OH)_2 \cdot mH_2O$ (*cf.* Table 3), characterised by an average x of 0.17 ± 0.04 (Fig. 8). The m parameter, *i.e.*, the amount of molecular H_2O derived from measured total H_2O, should be around 1.10 mol per for-

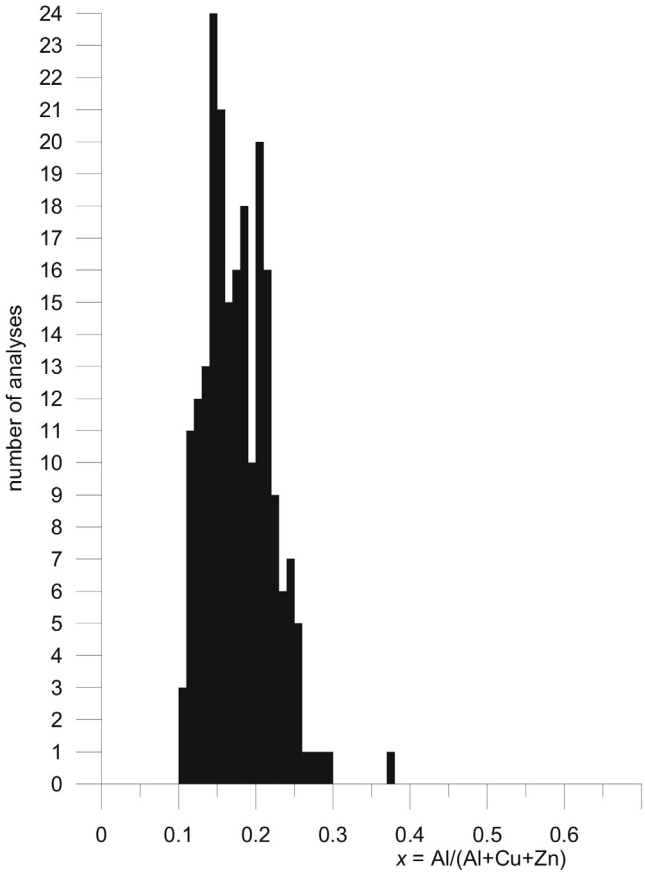

Fig. 8. Histogram of the composition of the analysed hydrowoodwardite (sample 1, *Eve verda*; see Appendix for the EMP analytical conditions).

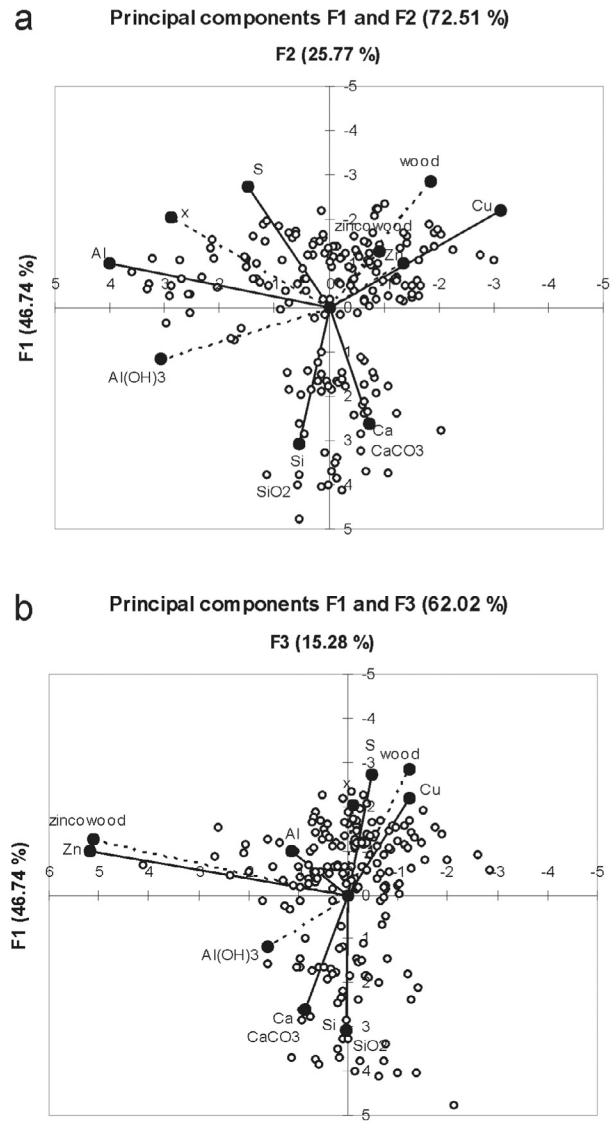

Fig. 9. Principal component analysis of the EMP data. Sample 1 of *Eve verda*; {[O], Al, Si, S, Ca, Cu, Zn}: original basis of the compositional vectorial space; {F1, . . . , F6}: principal components (*i.e.*, eigenvectors of the covariance matrix); $Al(OH)_3$, hydrowoodwardite (wood), zincowoodwardite (zincowood), SiO_2, $CaCO_3$ and *x*: vectors not considered in the statistics but displayed for reference (broken lines).

mula unit (Table 4), a value comparable to that of glaucocerinite (*cf.* Table 3).

In order to emphasise possible correlations in the chemical composition of the deposit, we carried out principal component analysis (PCA) on the EMP data (Fig. 9, Table 5). The main principal component F1 (relative eigenvalue of 46.7 %) counters hydrowoodwardite (*i.e.*, Zn+Cu+S) with the sum of $Al(OH)_3$ and SiO_2 ($+CaCO_3$). This component represents therefore the hydrowoodwardite *versus* Al–Si oxyhydroxides ratio, *i.e.*, deep *versus* light colouration of the precipitate. The principal component F2 (25.8 %) accounts for the richness in Al, which is expressed both by the *x* parameter of hydrowoodwardite [*i.e.*, Al/(Al+Cu+Zn)] and the abundance of $Al(OH)_3$. This F2 principal component mainly concerns the deep-coloured matter. The principal components F3 (15.3 %) and F4 (7.6 %) represent the abundance of Zn in hydrowoodwardite and of Ca in the precipitate, respectively. The latter components are of limited significance.

We also performed PCA on EDX elemental maps (Fig. 10, Table 5). Although the analytical techniques and the analysed points were different, the eigenvectors and eigenvalues of the covariance matrix are similar to those obtained from the previous EMP data (Table 5). The resulting image for the principal component F1 (Fig. 10) indicates that two types of flakes, with different richness in hydrowoodwardite, exist in the precipitate (A and B in Fig. 10). This bimodal distribution is also visible in Fig. 9, where a gap occurs for $0 < F1 < 1$. On the other hand, the F2 image emphasises the microlayering of the flakes with the occurrence of thin Al-rich and Cu-poor films at the former interface with water (R in Fig. 10). The F3 and F4 images represent, respectively, the distribution of Zn in hydrowoodwardite and Ca in the precipitate, as indicated

Table 5. Principal component analysis of the EMP and EDX chemical analyses of sample 1 (*Eve Verda*): Eigenvectors and eigenvalues of the covariance matrix.

Principal components	F1		F2		F3		F4		F5	
	EMP	EDX	EMP	EDX	EMP	EDX	EMP	EDX	EMP	EDX
Eigenvectors										
Cu	–0.398	–0.523	–0.566	–0.721	–0.220	–0.031	0.162	0.011	–0.125	–0.105
Zn	–0.178	–0.009	–0.249	–0.049	0.935	0.986	–0.134	0.078	0.111	0.138
Al	–0.182	–0.330	0.721	0.656	0.211	0.026	0.209	–0.003	–0.388	–0.019
S	–0.496	–0.069	0.268	–0.055	–0.088	–0.141	0.210	–0.015	0.794	0.985
Si	0.557	0.782	0.099	–0.211	–0.001	–0.010	–0.387	–0.010	0.416	0.010
Ca	0.470	0.013	–0.130	0.011	0.159	–0.079	0.848	0.997	0.130	0.005
Eigenvalues (%)	46.7	59.2	25.8	24.9	15.3	5.7	7.6	7.0	4.6	3.3

EMP: quantitative data from microprobe analyses; EDX: semiquantitative data from elemental X-ray maps.
The results of the principal component analyses are presented in Fig. 9 (EMP) and 10 (EDX).
Component F6 is in both cases non significant as the sum of the elements were normalised.

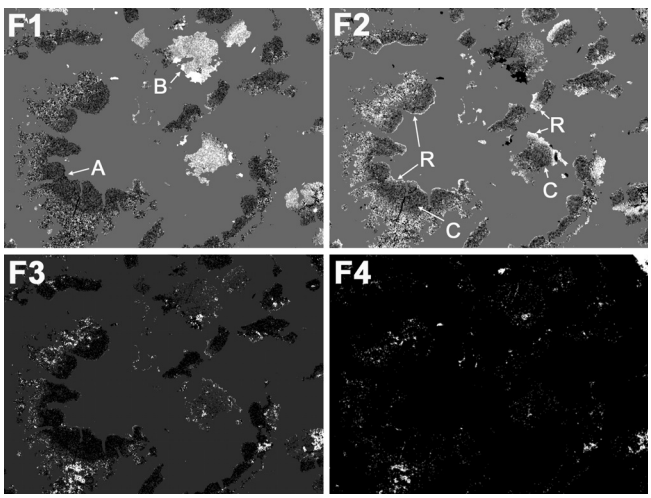

Fig. 10. Images of the principal components F1–F4 obtained from principal component analysis of elemental EDX maps. A and B are areas where F1 is low and high, respectively; C (core) and R (rim) are areas where F2 is low and high, respectively. Eigenvalues and eigenvectors of the covariance matrix are listed in Table 6. The analysed area is the same as in Fig. 6.

by the coordinates of these elements in the F3 and F4 eigenvectors (Table 5).

3.3. Discussion of the characterisation

Diffraction data and chemical analyses suggest that the blue-green precipitate is composed mainly of a nanocrystalline phase related to hydrowoodwardite, *i.e.*, a Cu–Al–sulphate hydrotalcite-like compound characterised by a variable Al/(Al+Cu) ratio, which ranges between 0.10 and 0.30 (average 0.17 ± 0.04) in our sample. The excess of Al and Si could be ascribed to admixed phases, such as amorphous Al and/or Si oxyhydroxides. The hydrowoodwardite *versus* Al–Si oxyhydroxides ratio is also variable, ranging from 0.23 to 0.64, and gives rise to a bimodal composition of the precipitate (see F1 in Fig. 9 and 10). This corresponds to a bimodal colouration of the precipitate, ranging from light to deep blue-green, and which could be due to seasonal cycles (Prosio, 1903). On the other hand, the effect of the Al/(Al+Cu) ratio in hydrowoodwardite on the colour remains uncertain.

In some samples of *Galleria Ribasso*, associated crystalline phases, such as malachite and hydrated sulphates, have been found as well.

4. Genesis of the precipitate

The genesis of Cu-bearing hydrotalcites has not yet been modelled, due to the lack of reliable thermodynamic data. In this section, we propose a thermodynamic modelling of hydrowoodwardite precipitation, and then discuss the physical and chemical conditions required for its genesis, considering *Eve Verda* as a case study.

4.1. Thermodynamic modelling

As reported by Allada *et al.* (2002), predictions of total metal concentrations in aquifers usually rely on the calculated solubilities of minerals with fixed composition, particularly on simple hydroxides, carbonates, sulphates and others, for which thermodynamic data are available. On the contrary, solids of variable composition, like hydrotalcites, are usually ignored because thermodynamic data are missing or difficult to acquire (Allada *et al.*, 2002, and references therein).

In the scientific literature, thermodynamic data measurements are reported only for Mg-, Zn-, Co- and Ni-bearing hydrotalcites. These data consist of:

(i) enthalpy of formation determined by calorimetry (Allada *et al.*, 2002; Peltier *et al.*, 2006; Allada *et al.*, 2006);

(ii) solubility product constant K_{sp} determined by solubility measurements (Johnson & Glasser, 2003).

The thermodynamic properties of Cu–Al–sulphate hydrotalcites (*i.e.*, hydrowoodwardite) are unknown, but they can be *estimated*, in three independent ways:

(i) estimating ΔG^0_f and ΔH^0_f using the model of Bravo-Suárez *et al.* (2004);

(ii) estimating ΔH^0_f of Cu-bearing hydrotalcites using those of Mg-, Zn-, Co- and Ni-bearing hydrotalcites, which Allada *et al.* (2002), Peltier *et al.* (2006) and Allada *et al.* (2006) have determined by calorimetry;

(iii) estimating ΔG^0_f of Cu-bearing hydrotalcites using solubility measurements carried out on Mg-, Zn-, Co- and Ni-bearing hydrotalcites by Johnson & Glasser (2003).

The thermodynamic data used in calculations and their references are reported in the Appendix (Tables Xa and b).

4.1.1. Model of Bravo-Suárez et al. (2004)

The model of Allada *et al*. (2002) and the improved one of Bravo-Suárez *et al*. (2004) are extensions of the Newmann-Kopp rule and follow the intuitions of Latimer (1951, 1952) and Fyfe *et al.* (1958), who used entropies of the elements and oxides, respectively, to estimate entropies of more complex compounds. In practice, Allada *et al.* (2002) estimated the enthalpy of formation of Mg–Al and Co–Al carbonate hydrotalcites by considering them as equivalent mechanical mixtures of binary hydroxides. The authors obtained good agreement between estimated and measured parameters. This mechanical-mixture approach is justified on the atomic scale because the metal and anion coordination environments in the hydrotalcite are structurally, and hence energetically, similar to those in the simple minerals used as components, *i.e.*, $M^{2+}CO_3$, $Al(OH)_3$, $M^{2+}(OH)_2$ and H_2O (Allada *et al.*, 2002).

The improved and generalised model of Bravo-Suárez *et al.* (2004) also treats hydrotalcites as mixtures of simple but structurally similar compounds, but, unlike the model of Allada *et al.* (2002), the authors consider several possible combinations among more terms [*i.e.*, $M^{2+}(OH)_2$, $M^{3+}(OH)_3$, A^{n-}, $H_n(A^{n-})$, $M^{2+}(A^{n-})_{2/n}$ and $M^{3+}_n(A^{n-})_3$], taking into account all of the possible interactions of the interlayer anions.

We used the model of Bravo-Suárez *et al.* (2004) to obtain ΔG^0_f and ΔH^0_f of sulphate hydrotalcites with variable values for x = Al/(Al+Cu). The points were interpolated by linear regression (Fig. 11), fixing the point for $x = 0$ whose properties are known experimentally (see $Cu(OH)_2$ in Table Xa). This interpolation gave the following relations:

$$\Delta G^0_f = -974.19 \cdot x - 357.70$$

$$\Delta H^0_f = -1041.91 \cdot x - 447.15.$$

Following this model, woodwardite *sensu stricto* (*i.e.*, a Cu–Al–sulphate hydrotalcite with $x = 1/3$), excluding the contribution of the hydration water (*i.e.*, $m = 0$), would be characterised by $\Delta G^0_f = -682.9$ kJ/mol and $\Delta H^0_f = -794.5$ kJ/mol (Table 6).

4.1.2. Analogue model from calorimetric data

Calorimetric determination of ΔH^0_f is still lacking for Cu-bearing hydrotalcites, while it is available for other M^{2+}-bearing species (*cf.* Allada *et al.*, 2002; Peltier *et al.*, 2006; Allada *et al.*, 2006). We tried to estimate ΔH^0_f of Cu-bearing hydrotalcite by subtracting the contributions of $M^{2+}(OH)_2$and $M^{2+}(A^{n-})_{2/n}$ to the measured ΔH^0_f of an M^{2+}–A^{n-}-bearing analogue and by adding the contributions of $Cu(OH)_2$ and $CuSO_4$. For example, starting from the measured ΔH^0_f of an analogue whose composition is $Ni_{0.64}Al_{0.36}(OH)_2(CO_3)_{0.18}\cdot 0.46\ H_2O$, we can obtain ΔH^0_f of the Cu–sulphate hydrotalcite $[Cu_{0.64}Al_{0.36}(OH)_2(SO_4)_{0.18} \cdot 0.46\ H_2O]$ in the following way:

$$\Delta H^0_{f\ Cu_{0.64}Al_{0.36}(OH)_2(SO_4)_{0.18}\cdot 0.46H_2O} =$$
$$\Delta H^0_{f\ Ni_{0.64}Al_{0.36}(OH)_2(CO_3)_{0.18}\cdot 0.46H_2O}$$
$$- 0.18\Delta H^0_{f\ NiCO_3} + 0.18\Delta H^0_{f\ CuSO_4}$$
$$- 0.46\Delta H^0_{f\ Ni(OH)_2} + 0.46\Delta H^0_{f\ Cu(OH)_2}.$$

The approach used is an extension of that of Helgeson *et al.* (1978), who applied the Newmann-Kopp rule taking structurally analogous mineral phases as components instead of simple oxides/hydroxides. This method lowers the number of components and minimises the differences in coordination state between these components and the phase "being built" so uncertainties are reduced.

Once we estimated the enthalpies of formation ($\Delta H^{0\,est}_f$), the free-energies of formation ($\Delta G^{0\,est}_f$; see Table 7) were calculated according to Peltier *et al.* (2006) on the basis of the relation:

$$\Delta G^{0\,est}_f = \Delta G^{end}_f + \Delta H^{0\,est}_f - \Delta H^{end}_f - T\Delta S^{scc},$$

where $T\Delta S^{scc}$ is the entropy contribution to the free energy (–1.9 kJ/mol at 298K, as for Mg hydrotalcite; see Allada *et al.*, 2005), and ΔG^{end}_f and ΔH^{end}_f are the free energies and enthalpies of formation calculated from those of the end-member components. For example, ΔH^{end}_f of the hydrotalcite $Cu_{0.64}Al_{0.36}(OH)_2(SO_4)_{0.18}\cdot 0.46\ H_2O$ can be calculated in the following way:

$$\Delta H^{end}_{f\ Cu_{0.64}Al_{0.36}(OH)_2(SO4)_{0.18}\cdot 0.46H_2O} = 0.46\Delta H^0_{f\ Cu(OH)_2}$$
$$+0.18\Delta H^0_{f\ CuSO_4} + 0.36\Delta H^0_{f\ Al(OH)_3} + 0.46\Delta H^0_{f\ H_2O}.$$

In order to derive a solid-solution model for Cu–Al–sulphate hydrotalcites, the obtained values of $\Delta G^{0\,est}_f$ were plotted as a function of x [*i.e.*, the Al/(Al+Cu) ratio]. Since these hydrotalcites can be represented as binary solid-solutions of the two end-members $Cu(OH)_2$ (spertiniite: sp; $x = 0$) and a theoretical compound $Al(OH)_2(SO_4)_{0.5}$ (aluminite: al; $x = 1$), the free-energy of formation for each Cu hydrotalcite (HTlc) could then be written using the following expression (*cf.* Bourrié *et al.*, 2004; and Peltier *et al.*, 2006 for Ni hydrotalcites):

$$\Delta G^0_{f\ HTlc} = (1 - x) \cdot \Delta G^0_{f\ sp} + x \cdot \Delta G^0_{f\ al} + \Delta G^0_{mix},$$
$$\Delta G^0_{mix} = \Delta G^0_{mix,ideal} + A_0 \cdot x \cdot (1 - x),$$
$$\Delta G^0_{mix,ideal} = RT \cdot [(1 - x) \cdot \ln(1 - x) + x \cdot \ln(x)].$$

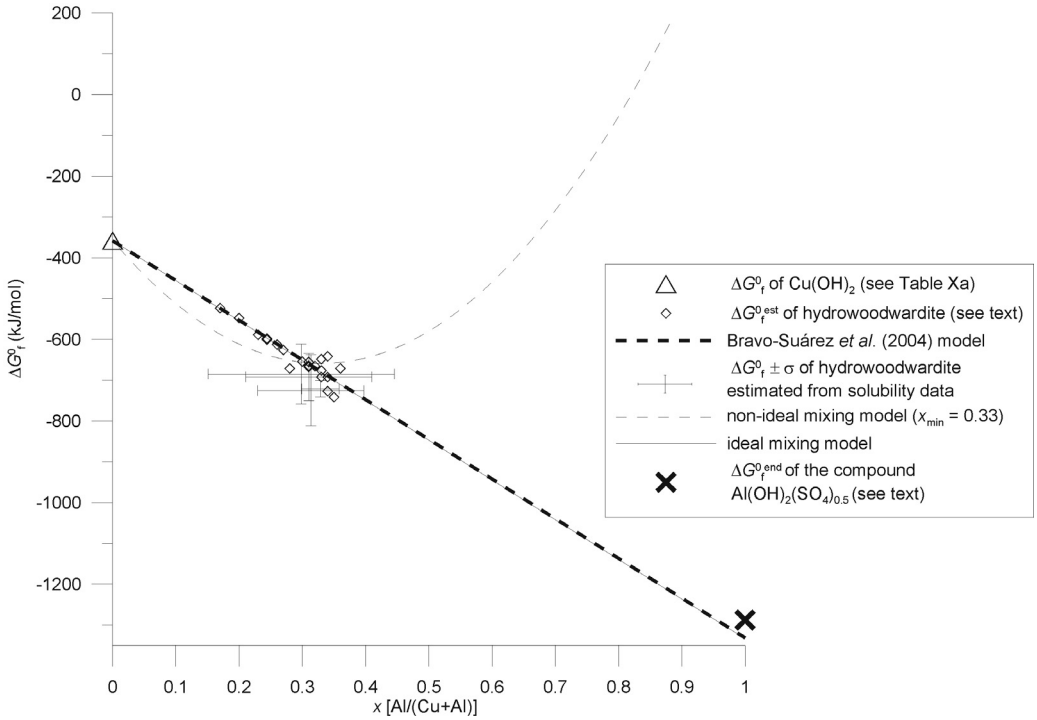

Fig. 11. Diagram of Gibbs free energy of formation *versus* x for hydrowoodwardite solid solution. The different fitting models are displayed for reference (see text for details).

In the case of ideal mixing A_0 is null, whereas in the case of non-ideal mixing:

$$A_0 = [\Delta G^0_{\mathrm{f\ sp}} - \Delta G^0_{\mathrm{f\ al}} + RT \cdot \ln(x_{\min}/(1-x_{\min}))]/(1-2x_{\min}),$$

where $x_{\min}$ is the value of x that minimises the free energy of formation.

The $\Delta G^{0\,\mathrm{est}}_{\mathrm{f}}$ values (Table 6) could be fitted either assuming ideal or non-ideal mixing models.

If one considers a non-ideal mixing model similar to that proposed by Peltier *et al.* (2006), ΔG^0_{f} depends on a chosen $x_{\min}$ value (see above). We assumed $x_{\min} = 0.33$ because several studies have indicated that beyond a value of $x = 0.33$–0.35, increased Al substitution results in the formation of localized $Al(OH)_3$ islands in the sample rather than a consistent solid solution (Peltier *et al.*, 2006, and references therein). This is supported by the vast majority of hydrotalcite literature, in which natural or synthesized samples containing $x > 0.4$ are very rare (Brindley & Kikkawa, 1979). According to this model, a hydrotalcite with woodwardite stoichiometry ($x = 1/3$) would be characterised by $\Delta G^0_{\mathrm{f}} = -658.6$ kJ/mol, a value 3.56 % higher than that obtained with the Bravo-Suárez model (Fig. 11). The non-ideal mixing model provides $\Delta G^0_{\mathrm{f}} = +573.3$ kJ/mol for the compound $Al(OH)_2(SO_4)_{0.5}$, which therefore has to be considered only a theoretical unstable end-member ($x = 1$) of the hydrowoodwardite solid solution (see also Peltier *et al.*, 2006).

The ideal mixing model fits the $\Delta G^{0\,est}_{\mathrm{f}}$ data as well (Fig. 11), so it could be used conveniently for hydrowoodwardite at least for x values below ≈ 0.35 (see above). It should be emphasised that the ideal model remarkably reproduces the one of Bravo-Suárez *et al.* (2004). Following this model, a hydrotalcite with woodwardite stoichiometry (*i.e.*, $x = 1/3$) would be characterised by $\Delta G^0_{\mathrm{f}} = -684.4$ kJ/mol and $\Delta H^0_{\mathrm{f}} = -795.0$ kJ/mol. This model provides negative ΔG^0_{f} and ΔH^0_{f} values for the compound $Al(OH)_2(SO_4)_{0.5}$ (–1333.1 and –1486.0 kJ/mol, respectively) that are close to $\Delta G^{\mathrm{end}}_{\mathrm{f}}$ and $\Delta H^{\mathrm{end}}_{\mathrm{f}}$ calculated by adding 2/3 of $Al(OH)_3$ and 1/6 $Al_2(SO_4)_3$ ($\Delta G^{\mathrm{end}}_{\mathrm{f}} = -1287.7$ and $\Delta H^{\mathrm{end}}_{\mathrm{f}} = -1435.7$ kJ/mol) (Fig. 11).

In conclusion, the ideal mixing model and the non-ideal model differ only slightly for $x < 0.4$ and therefore also for the compositions of hydrowoodwardite occurring at *Eve verda* (*i.e.*, $x < 0.3$; Fig. 8). However, the fact that natural and synthesised hydrowoodwardite seems to display a compositional gap beyond $x \approx 0.33$–0.35 points towards a non-ideal behaviour of this solid solution. A major doubt remains concerning the end-member $Al(OH)_2(SO_4)_{0.5}$. Because the copper solubility in aluminite has not been experimentally investigated, it is not clear whether this compound should be considered either a theoretical or a stable end-member of a spertiniite–aluminite solid solution characterised by a large solvus.

4.1.3. Cu-analogue model from solubility data

The ΔG^0_{f} of hydrotalcites can also be derived from measured solubility-product constants (K_{sp}). To the best of

Table 6. Estimated thermodynamic data for hydrowoodwardite ($Cu_{1-x}Al_x(OH)_2[SO_4]_{x/2}$).

Models/references	Originary M^{2+}	Originary A^{n-}	x	σ	$\Delta G_f^{0\,est}$	σ	$\Delta H_f^{0\,est}$	σ
from experimental data								
Johnson & Glasser (2003)	Mg	CO_3	0.31	0.08	–725.0	–87.5	-	-
	Zn	CO_3	0.33	0.03	–721.2	–20.3	-	-
	Co	CO_3	0.30	0.15	–685.3	–73.5	-	-
	Ni	CO_3	0.31	0.1	–692.1	–57.8	-	-
Peltier *et al.* (2006)	Ni	SO_4	0.34	-	–726.9	1.6	–837.6	1.6
	Ni	SO_4	0.35	-	–741.7	1.9	–852.9	1.9
	Ni	SO_4	0.28	-	–671.3	1.7	–778.6	1.7
	Co	CO_3	0.32	-	–665.4	2.5	–775.0	2.5
	Co	CO_3	0.24	-	–597.8	1.7	–703.0	1.7
	Co	CO_3	0.24	-	–600.8	3.3	–706.1	3.3
Allada *et al.* (2002)	Co	CO_3	0.31	-	–655.2	1.6	–764.4	1.6
	Co	CO_3	0.30	-	–654.4	1.4	–763.1	1.4
	Co	CO_3	0.20	-	–547.7	2.2	–650.5	2.2
Allada *et al.* (2006)	Co	CO_3	0.17	-	–523.2	2.0	–624.4	2.0
	Mg	CO_3	0.33	-	–676.6	1.8	–786.6	1.8
	Mg	CO_3	0.34	-	–692.3	1.6	–803.1	1.6
	Mg	CO_3	0.31	-	–665.0	1.8	–773.9	1.8
	Mg	CO_3	0.26	-	–612.8	2.1	–719.0	2.1
	Mg	CO_3	0.27	-	–626.1	2.0	–733.4	2.0
	Ni	CO_3	0.31	-	–667.4	1.2	–776.5	1.2
	Ni	CO_3	0.34	-	–641.7	0.9	–752.4	0.9
	Ni	CO_3	0.23	-	–588.6	1.3	–693.2	1.3
	Ni	CO_3	0.33	-	–648.4	2.1	–758.7	2.1
	Ni	CO_3	0.36	-	–671.1	1.5	–783.0	1.5
	Zn	CO_3	0.33	-	–692.6	1.0	–802.9	1.0
from mixing models								
Bravo-Suárez *et al.* (2004)	Cu	SO_4	0.33	-	–682.9	-	–794.5	-
ideal	Cu	SO_4	0.33	-	–684.4	-	–795.0	-
non-ideal	Cu	SO_4	0.33	-	–658.6	-	–767.5	-

ΔG_f^0 and ΔH_f^0 are Gibbs free energies of formation and enthalpies of formation from the elements.

our knowledge, direct solubility measurements carried out on well-characterised Cu–Al–sulphate hydrotalcites have never been published. Therefore, we derived ΔG_f^0 of Mg-, Zn-, Co- and Ni-hydrotalcites containing Al and CO_3^{2-} from their solubility products measured by Johnson & Glasser (2003). Then, we estimated ΔG_f^0 for the analogue Cu–sulphate hydrotalcite in the same manner outlined in Section 4.1.2. The uncertainties of the compositions of the phases and of K_{sp} produce a high degree of uncertainty of ΔG_f^0 and x (up to 12.06 % and 49.44 %, respectively; Fig. 11). However, the estimated values of ΔG_f^0 are comparable with the results of the previously seen models.

4.2. Phase diagrams

The thermodynamic modelling of the Cu–S–Al–Si–H–O ± CO_2 system was performed with the software Domino V.140205 by Christian de Capitani (http://titan.minpet.unibas.ch/minpet/theriak/theruser.html; see also de Capitani & Brown 1987) and a thermodynamic database compiled *ad hoc* (Tables 6, Xa and Xb). Although this software is used traditionally to solve petrological problems, we chose it instead of more classic geochemistry-oriented software (for example, PHREEQ, EQ3/6, MINTEQ), for the following reasons:

(i) it allows fixing the composition of the system instead of the composition of the water only, allowing the calculation of real pseudosections, *i.e.*, isochemical phase diagrams valid only for a fixed composition of the system (Hensen, 1971; Hensen & Green, 1971);
(ii) it automatically draws $Y - Y'$, $Y - X$ and $X - X'$ pseudosections, where Y and Y' are external intensive variables [such as P, T, pH, $a(CO_2)$] and X, X' internal extensive compositional properties;
(iii) it deals easily with solid solutions, drawing optionally isolines (*e.g.*, isopleths, isomodes, *etc.*) on the calculated diagrams.

In order to render the thermodynamic modelling possible, we adopted a few assumptions that simplified the problem:

(i) the calculated equilibria involves a selection of solid phases: (a) hydrowoodwardite, *i.e.*, the solid solution $Cu_{1-x}Al_x(SO_4)_{x/2}(OH)_2$ with $0 < x < 0.33$ (see Sect. 4.1.2) and $m = 1$; (b) malachite; (c) gibbsite;

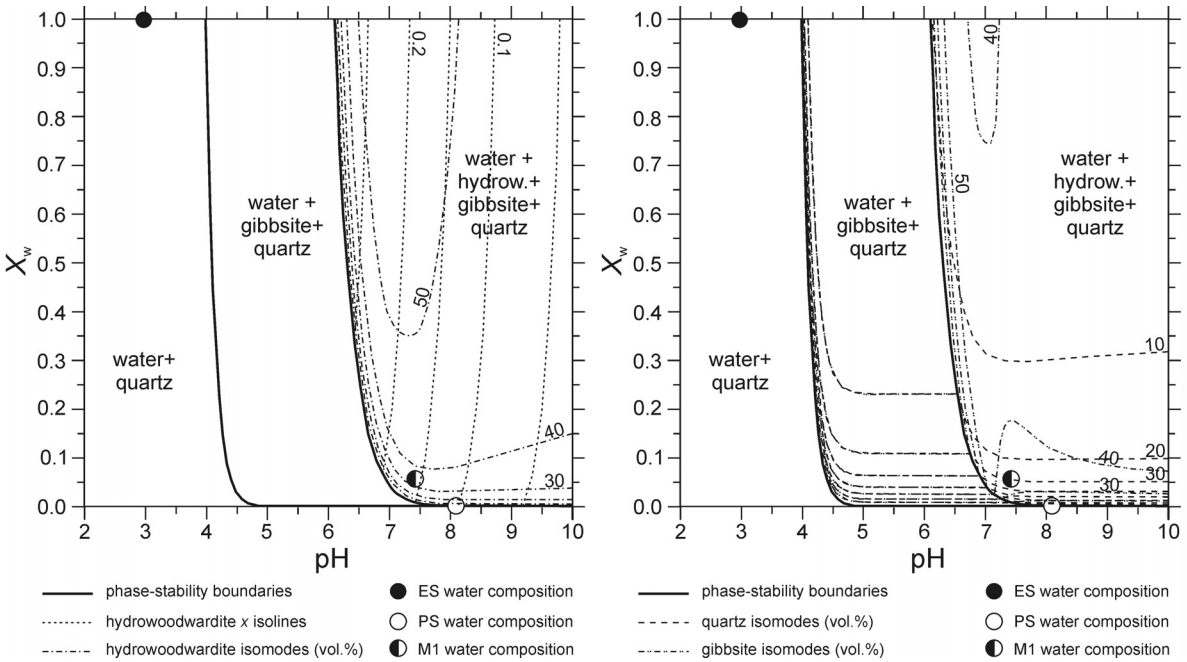

Fig. 12. pH *versus* X_w phase diagrams in the system Cu–S–Al–Si–H–O at T = 5.8 °C and P = 1 bar. X_w is the molar proportion of the two mixing waters (i) ephemeral-stream waters (ES, X_w = 1) and (ii) perennial-spring waters (PS, X_w = 0). The composition of mixed water (M1) is also displayed for reference. Isomodes are expressed in volume % of the precipitate.

(d) quartz; (e) other Cu-phases such as chalcocyanite ($CuSO_4$), dioptase ($CuSiO_3{\cdot}H_2O$) and chrysocolla ($CuSiO_3{\cdot}2H_2O$). The thermodynamic data used in calculations are reported in the Appendix (Tables Xa and Xb);

(ii) we simplified the speciation of the elements dissolved into the water solution; in practice, we considered water as an ideal solution composed of Al^{3+}, $Al(OH)_4^-$, CO_2 (aqueous), Cu^{2+}, $Cu(OH)^-$, $H_4SiO_4^0$, SO_4^{2-}, H^+ and H_2O (liquid);

(iii) although the average pressure at an altitude of 1370 m is 0.859 bar, P was constrained to 1 bar because the available thermodynamic data refer to the standard state at 1 bar.

(iv) T was fixed at 5.8 °C, the value reported in Table 1 for the water M1, where sample 1 was collected.

For the system Cu–S–Al–Si–H–O, a pH *versus* X_w pseudosection was calculated (Fig. 12), where X_w corresponds to the molar proportions in the mixture between the waters of the ephemeral (ES) and the perennial (PS) springs. Figure 13 also shows a pH *versus* log $a(CO_2)$ pseudosection for the same system with added carbon dioxide.

4.2.1. The system Cu–S–Al–Si–H–O

The blue-green matter precipitates from water M1, which is probably related to a mixture of the ephemeral stream (ES) and perennial spring (PS) waters (see Sect. 2.2). In order to verify this hypothesis, we performed a mass balance using the least-square algorithm, and considering 5 independent constituents (Cu, S, Al, Si, H; O was deduced by stoichiometry). The calculation indicates that the composition of M1 may be expressed as a linear combination of the molar composition vectors of three components: ES, PS, and the blue-green deposit (D):

$$0.941 \cdot \mathrm{PS} + 0.058 \cdot \mathrm{ES} = 1 \cdot \mathrm{M1} + 1.444 \times 10^{-5} \cdot \mathrm{D} + R \quad \text{(eq.1)},$$

where the vector R is the residual of the least-square regression. This implies a precipitation of 14.44 g of blue-green matter (D) per 1 m^3 of water (M1). Very close results are obtained using the composition of the nearby M2 water (Fig. 1, Table 1).

In order to explain the precipitation in this context, we constructed a pH–X_w pseudosection, where X_w is the ES/PS ratio in the water mixture (Fig. 12). Both the ES and PS water compositions fall in hydrowoodwardite-free fields, whereas the mixed M1 water composition falls in the field water + gibbsite + quartz + hydrowoodwardite, explaining the precipitation of the blue-green material. We also calculated the following isolines: (i) x [=Al/(Al+Cu)] isopleths in hydrowoodwardite; (ii) isomodes, *i.e.*, isolines of the phase abundances in the precipitate expressed in vol.% (Fig. 12). This provides the theoretical composition of the precipitate at equilibrium with the M1 water ($x \approx 0.16$, hydrowoodwardite ≈ 34 vol.%, $Al(OH)_3$ ≈ 35 vol.%, SiO_2 ≈ 31 vol.%), which can be compared with the effective composition of the precipitate ($x \approx 0.17$, hydrowoodwardite ≈ 49 vol.%, gibbsite ≈ 31 vol.%, quartz ≈ 19 vol.%; Table 4).

4.2.2. The system Cu–S–Al–Si–H–O + CO_2

Figure 13 presents a pH *versus* log $a(CO_2)$ pseudosection for the system Cu–S–Al–Si–H–O + CO_2. This was calculated for X_w = 0.058, *i.e.*, the ES/PS ratio that characterises

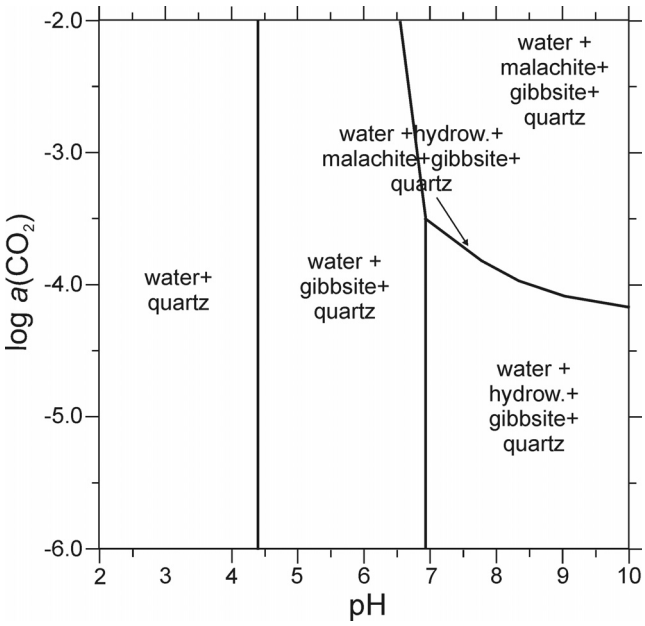

Fig. 13. pH *versus* log $a(CO_2)$ phase diagram in the system Cu–S–Al–Si–H–O + CO_2 at T = 5.8 °C and P = 1 bar. The system composition is that of the mixed water M1 (*i.e.*, X_w = 0.058).

the M1 water (Eq. (1)). We found a univariant curve that represents the stability of hydrowoodwardite against malachite. At pH = 7.4, malachite would become stable for log $a(CO_2) > -3.7$, *i.e.*, $[CO_2] > 2 \times 10^{-4}$ mol/L.

4.3. Discussion of the genesis

The thermodynamic modelling yields a pH–X_w pseudosection (Fig. 12) that accounts well for the precipitation of the blue-green deposit. While the two non-mixed waters (*i.e.*, PS and ES) lie in a hydrowoodwardite- and gibbsite-free field, the water that results from their mixing (*i.e.*, M1) lies onto the field water + hydrowoodwardite + gibbsite + quartz.

A comparison between the PCA biplot of the real precipitate (Fig. 9) and the pseudosection (Fig. 12) shows that the compositional vectors in Fig. 9 (x, $Al(OH)_3$, SiO_2, and hydrowoodwardite) are more or less perpendicular to the corresponding isolines in Fig. 12. This suggests that the modelling not only accounts for the precipitation of the blue-green deposit but also for the chemical variations observed in it. In particular, the F1 principal component correlates strongly with X_w. As the ES water flows only during summer, the ratio between the ES and PS waters (X_w) is probably subject to seasonal variations, explaining the bimodal composition of the precipitate (see F1 in Fig. 9 and 10). In other terms, the flakes A and B of Fig. 10 would have deposited during summer and winter, respectively. On the other hand, the F2 principal component is anticorrelated with pH, indicating that the microlayering of the blue-green matter (C and R in Fig. 10) is likely due to oscillations in pH.

The pH–CO_2 pseudosection (Fig. 13) suggests that hydrowoodwardite cannot precipitate from water with high-CO_2 activity. In this case, other phases would form, such as malachite, or possibly other carbonate-bearing hydrotalcites, such as carbonate-cyanotrichite (see Stara *et al.*, 1999). The occurrence of malachite in the encrustations of the upper *Galleria Ribasso* may be explained by a higher CO_2-content in the circulating water. Interestingly, carbonate-bearing calcschists occur close to this gallery (Fig. 1).

The modelling, however, is not totally satisfactory as differences appear between calculated isolines, especially isomodes, and the observed composition of the blue-green precipitate (see Fig. 12 *versus* Table 4). This could be ascribed to uncertainties related to the thermodynamic data/models and/or the water compositions.

The most critical uncertainties regarding thermodynamic modelling are related to hydrowoodwardite, whose thermodynamic properties were estimated instead of being experimentally determined. Particularly, we noticed a marked effect on the isomodes of the parameter m (*i.e.*, the degree of hydration of hydrowoodwardite); the higher the m parameter, the higher the abundance of hydrowoodwardite in the precipitate. On the other hand, the x isopleths fit the data well, suggesting good adequacy of the solid-solution model. Other sources of uncertainty are the presence of hypothetical phases in the precipitate that were not considered, such as kaolinite, the incomplete ion-speciation model for the water solution, and uncertainties on the thermodynamic data taken from the literature.

As for the water, the considered composition could be slightly different to the one from which the studied blue-green deposit effectively precipitated, as it is subject to seasonal and spatial variations. Moreover, some uncertainties on the content of certain elements in the water exist. Part of Al, for example, could be related to unfiltered microparticles in suspension (< 0.22 μm, *i.e.*, the mesh size of the filters), rather than truly dissolved Al ions. In fact, we noticed that dividing the Al content by 2 in water, yields isomodes for hydrowoodwardite and gibbsite closer to the observed data. Increasing the Cu content by 60 % also provides isomodes in good agreement with the observed precipitate composition.

5. General discussion

Hydrotalcites are compounds that recently attracted the attention of the international scientific community. In the last 10 years, we witnessed a constant increment of articles concerning hydrotalcites, the majority of which has been published by physical chemists. Hydrotalcites containing heavy metals have been proven to contribute to decreasing the content of these pollutants in waters, due to their low solubility (*cf.* Gade *et al.*, 2001, and references therein) and their ability to form directly on precipitated Al-hydroxide (*cf.* Thompson *et al.*, 1999). Recent studies suggest a higher

thermodynamic stability of Ni-bearing hydrotalcites compared to Ni-bearing oxides, hydroxides and carbonates (Allada *et al.*, 2006).

Cu–Al-rich hydrotalcite species, particularly those containing the anion SO_4, are known to occur in nature (Table 3), where they are probably more important than previously imagined. Because of the chemical similarity of Cu^{2+} with Zn^{2+} and Ni^{2+}, solid solutions between Cu-, Zn- and Ni-bearing Al-hydrotalcites also exist (*e.g.*, Nickel, 1976; Raade *et al.*, 1985; Witze, 1999). The attribution of these Cu–Al-rich hydrotalcites to a specific species, however, is often far-fetched since it is based typically on mediocre XRD data (see Sect. 3.1.2) and mixed chemical analyses. Until recently, they were often referred to with the ambiguous name "woodwardite".

In this section, we present an overview of "woodwardites" in the environment and discuss the contribution of our study to this question.

5.1. History and occurrence of "woodwardite"

The first description of a Cu–Al–sulphate hydrotalcite is probably just that of *Eve verda*, which Bertrand de Lom (1844) called *chalcogélide*, a name that was never adopted by the scientific community. Actually, the discovery of "woodwardite" is attributed to A.H. Church (1866a and b), who named the new mineral after the palaeontologist S.P. Woodward. The studied sample came from the collection of Richard Talling, a mineralogist from Lostwithiel (Cornwall). However, this mineral was still regarded as doubtful by Hintze (1930) because its chemical and physical characters were not well documented.

Meixner (1940) found a similar mineral in the Montefondoli-Pfunderer mine near Chiusa-Klausen (South Tyrol, Italy). He provided XRD data for the first time for both "woodwardite" from Cornwall and the mineral from South Tyrol, concluding that the observed minerals belonged to the same species, although characterised by broad, diffuse Debye-Scherrer rings. Weil *et al.* (1975) reported the occurrence of "woodwardite" at the Château mine (Urbeis, France), the diffraction pattern of which was similar to that of "A.S.T.M. 17-132", a diffraction pattern with a few lines also obtained in 1965 from a specimen sampled at Simdde Dallhuan (Drws-y-coed, Nantlle, Caernarvonshire, United Kingdom). Nickel (1976) was the first to understand that this mineral should not be labelled as "woodwardite". Raade *et al.* (1985) suggested that it could rather be considered the Cu-analogue of glaucocerinite, another Al-hydrotalcite mineral (see Table 4). A similar "woodwardite" was also reported from Craignure (Scotland) by Livingstone (1990), who suggested considering the Scottish and the Welsh samples as the Cu–Al analogue of hydrohonessite.

A mineral with a "woodwardite" stoichiometry, but a different XRD pattern, was found in the Festival deposit (eastern Siberia) (Yakhontova *et al.*, 1981). At Calamita (Elba Island, Italy), Göske *et al.* (1997) observed "woodwardite" as a spring-water precipitate. In a similar setting, Dinelli *et al.* (1998) found fine-grained deposits in the Vigonzano mine (Italy) that they attributed to a phase related to the woodwardite group, precipitating from neutral waters with a pH of ≈ 7.1. Dinelli & Tateo (2001, 2002) attributed this "woodwardite" precipitation to an alkaline geochemical barrier that thus controls the heavy-metal dispersion in solution. Another reported site in Italy is the Funtana Raminosa mine (Gadoni, Sardinia) (Frau *et al.*, 1998; Stara *et al.*, 1999), where "woodwardite" seems to crystallise after halloysite and before credite + carbonate-cyanotrichite. Green and blue biogenic materials, displaying analogies with the "Caernarvonshire woodwardite" and a stromatolite-like microtexture, were also described by Watanabe *et al.* (2003) at the Dogamaru mine (Shimane prefecture, Japan), where they precipitate from drainage waters with pH 6.0–6.6.

Witzke (1999), whose study concerns some findings in Saxony, tried to bring some order to the confusion that was "woodwardite", by proposing a general formula with variable Cu/Al ratio and re-naming the corresponding mineral as "hydrowoodwardite". One year later, he also defined zincowoodwardite, a Zn-dominant, Cu-bearing hydrowoodwardite, found in Laurion (Greece; Witzke & Raade, 2000). Zincowoodwardite was soon recognised to be a constituent of Bavarian hazardous waste landfills by Gade *et al.* (2001). Recently, Schubert *et al.* (2005) continued extending the reported occurrences of woodwardite-related minerals, as they found zincowoodwardite in a spring percolating through some ore-processing slags, supporting the environmental importance of this mineral and related phases.

Therefore, the occurrence of hydrowoodwardite at *Eve verda* belongs to a series of findings related to weathering in mining areas, precipitating from waters generally characterised by near-neutral pH.

5.2. Extended implications

Our study on hydrowoodwardite at *Eve verda* could suggest some more general conclusions about Cu-bearing hydrotalcites and their occurrence.

Hydrowoodwardite is a phase constituting mainly precipitates in mine waters. Although it displays a wide stability field, as demonstrated by thermodynamic modelling, its formation requires high contents of metals in water solution, in particular Cu and Al. Generally, these elements can be carried by waters that are weathering Cu-sulphide mineralizations hosted by Al-bearing rocks, lowering their pH and thus sustaining the occurrence of Al and Cu in their ionic form. However, hydrowoodwardite cannot form directly in strongly acidic waters. Especially if the water contains relatively low quantities of dissolved Cu (say, $[Cu] < 10^{-5}$ mol/L), high pH conditions ($pH \geqslant 7$) are required. These conditions can take place easily when mineralised mine waters mix with more diluted, alkaline surface waters. Finally, alkaline geochemical barriers (*sensu* Perel'man, 1986) appear to be the most reliable genetic environment for hydrowoodwardite and transition metal-bearing hydrotalcites in general.

Thermodynamic modelling also shows that the x parameter of hydrowoodwardite [*i.e.*, Al/(Al+Cu)] decreases as pH increases, approaching the end-member composition $Cu(OH)_2$ ($x = 0$) only for very alkaline solutions (pH ≈ 9–10), which are uncommon in nature. This model seems to be supported both by experimental studies (Babèan & Ševc, 1973) and by the relative higher abundance in nature of high-x compared to low-x hydrowoodwardite. Pure $Cu(OH)_2$ is extremely rare: spertiniite has been described without uncertainty only once in the Jeffrey mine, Quebec (Canada), precipitating from solutions characterised by pH = 9.2 (Grice & Gasparrini, 1981).

Equilibrium-thermodynamic calculations show that chrysocolla, a mineral frequently cited in the scientific literature but whose definite presence is often doubtful, seems to be thermodynamically unstable compared to the assemblage hydrowoodwardite + quartz. This agrees well with the observations of Cheah *et al.* (2000), who found that the sorption product of Cu^{2+} on amorphous silica is solid $Cu(OH)_2$ and not a copper silicate. In fact, the believed widespread occurrence of amorphous chrysocolla could well be erroneous, as most of the findings may actually be mixtures of amorphous silica and Cu-bearing hydrotalcites. This question cannot be solved using conventional methods, because chrysocolla occurs always as an amorphous phase, and in most cases, hydrowoodwardite as well (see Sect. 3).

Another interesting aspect of the study is the stability of hydrowoodwardite compared to malachite (Fig. 13). Hydrowoodwardite should form only for low-CO_2 water concentrations ($[CO_2] < 10^{-4}$ mol/L). Generally, the concentration of CO_2 in surface waters corresponds more or less to the CO_2 activity in the atmosphere, *i.e.*, $[CO_2] \approx 10^{-3}$ mol/L (*e.g.*, Faure, 1998). Therefore, in aerated surface environments, malachite should be more thermodynamically stable than hydrowoodwardite in most cases. In fact, hydrowoodwardite is generally an unusual mineral with respect to malachite. However, hydrowoodwardite and related phases have been found relatively often in nature. We suggest, as a general rule, that hydrowoodwardite can form in waters with relatively low CO_2content. Good candidates of such waters may be small watercourses, which might not have reached equilibrium with the atmosphere, preferably circulating on carbonate-free rocks.

6. Conclusion

A multidisciplinary approach has been followed for this study to explain the occurrence of Cu-bearing hydrotalcites, chiefly hydrowoodwardite, and their importance for the environment. In particular, we emphasise that:

(i) hydrowoodwardite occurs mainly as poorly crystalline precipitates from mine waters, as the formation of this mineral requires relatively high contents of Cu, Al and S in water solution;
(ii) it is stable only at high pH conditions (⩾ 6–7) that are quite uncommon in mine drainage waters weathering sulphides, so that other phenomena are required, such as mixing with not mineralised, alkaline waters;
(iii) the Al/(Al+Cu) ratio of hydrowoodwardite (x) depends mainly on the pH of the water from which the mineral precipitates, so that it could be considered a natural pH-meter;
(iv) hydrowoodwardite is more thermodynamically stable than malachite only for water CO_2-activities ⩽ 10^{-4}, whereas the assemblage hydrowoodwardite + silica is always stable over chrysocolla and other Cu-silicates.

This study has also some methodological results. We emphasise the suitability of techniques used in petrology and chemistry to environmental sciences. $X-Y$ pseudosections, in particular, are modelled phase diagrams, with isomodes and isopleths, in which X and Y are two compositional or external (P, T, pH,...) variables, all other parameters being fixed (see Sect. 4.2). Applied to any composition of interest, they may have interesting applications in environmental sciences. Principal component analysis can also reveal microstructures (see Fig. 10), which in turn can be correlated to some chemical or physical processes (see Sect. 4.3).

Acknowledgements: The authors are indebted to Sonia Mosconi (CHN analysis, University of Insubria), Omar Boudouma (SEM, University of Paris) and Michel Fialin (electron microprobe, University of Paris) for technical assistance. They also appreciate the useful suggestions of Roberto Gambillara, Silvia Terrana and Elena Ciceri (University of Insubria) concerning water chemistry and hydrogeology of the Saint-Marcel valley. Nancy Mammi is thanked for the English corrections. The study was sponsored by the Saint-Marcel municipality within the project INTERREG IIIA 2000-2006 Italy-France (ALCOTRA) and partially funded by ERDF funds in the framework of the EU Community Initiative INTERREG III B Alpine Space Programme - project IRON ROUTE. S.T. was supported by a fellowship given by the *Istituto della Montagna* (ex INRM, Rome, Italy). The manuscript benefited from helpful suggestions of the reviewers E. Dinelli, P. Lattanzi and E. Peltier, who are gratefully acknowledged.

Appendix: Analytical methods

Blue-green precipitate samples were dried at room temperature and gently ground in an agate mortar before instrumental determinations.

Powder X-ray diffraction data (Cu$K\alpha$, $\lambda = 1.5418$) were collected on a θ:θ Bruker AXS D8 diffractometer equipped with primary and secondary Soller slits (2.3°), divergence, antiscatter, and receiving slits (0.5°, 0.5°, and 0.2 mm, respectively), secondary beam curved graphite monochromator, Na(Tl)I scintillation detector, and pulse height amplifier discrimination. The generator was operated at 40 kV and 40 mA.

Chemical analysis of the blue-green matter was performed using the Cameca SX100 wavelength dispersive electron microprobe (EMP) of the University of Paris. The dried powdery sample was enclosed in epoxy resin, polished and carbon-coated to prevent charging. Operating

Table Xa. $\Delta G_f 0$ and ΔH_f^0 data used in calculations, with references.

	ΔG_f^0 (kJ/mol)	Reference	ΔH_f^0 (kJ/mol)	Reference
H_2O (l)	–237.20	Robie & Hemingway (1995)	–285.83	Robie *et al.* (1979)
H^+	0.00	Robie *et al.* (1979)	0.00	Robie *et al.* (1979)
CO_2	–394.38	Robie *et al.* (1979)	–393.51	Robie *et al.* (1979)
CO_3^{2-}	–527.90	Faure (1998)	–677.10	Bravo-Suárez *et al.* (2004)
$H2CO_3^0$	–623.16	Faure (1998)	–699.65	Faure (1998)
SO_4^{2-}	–743.90	Bravo-Suárez *et al.* (2004)	–909.88	Faure (1998)
$H_2SO_4^0$	–743.71	Faure (1998)	–909.27	Faure (1998)
H_4SiO_4	–1307.70	Johnson *et al.* (1992)	–1449.40	Johnson *et al.* (1992)
SiO_2 (am)	–851.30	Faure (1998)	–904.10	Faure (1998)
Al^{3+}	–489.40	Faure (1998)	–531.00	Faure (1998)
gibbsite	–1156.90	Bravo-Suárez *et al.* (2004)	–1293.34	Allada *et al.* (2002)
$Al_2(SO_4)_3$	–3098.29	Robie *et al.* (1979)	–3440.84	Robie *et al.* (1979)
$MgCO_3$	–1029.68	Faure (1998)	–1113.36	Faure (1998)
$Mg(OH)_2$	–833.60	Bravo-Suárez *et al.* (2004)	–925.25	Faure (1998)
$NiCO_3$	–612.10	Peltier *et al.* (2006)	–689.10	Peltier *et al.* (2006)
β-$Ni(OH)_2$	–459.10	Allada *et al.* (2006)	–540.34	Allada *et al.* (2006)
$NiSO_4$	–873.20	Allada *et al.* (2006)	–762.70	Allada *et al.* (2002)
$CoCO_3$	–651.34	Faure (1998)	–745.82	Allada *et al.* (2002)
β-$Co(OH)_2$	–455.60	Bravo-Suárez *et al.* (2004)	–544.70	Allada *et al.* (2002)
$ZnCO_3$	–732.06	Faure (1998)	–812.78	Robie & Hemingway (1995)
$Zn(OH)_2$	–554.50	Bravo-Suárez *et al.* (2004)	–642.00	Allada *et al.* (2006)
Cu^{2+}	65.52	Faure (1998)	64.81	Faure (1998)
$Cu(OH)_2$ (s)	–357.70	Bravo-Suárez *et al.* (2004)	-447.15	Faure (1998)
$CuSO_4$ (s)	–661.91	Faure (1998)	–771.36	Faure (1998)
quartz	–910.94	Johnson *et al.* (1992)	–856.64	Johnson *et al.* (1992)
dioptase	–1208.31	Faure (1998)	–1359.87	Faure (1998)
chrysocolla	–1443.90	Faure (1998)	–1645.70	estimated (dioptase + H_2O)
malachite	–893.70	Weast (1985)	–1051.44	Weast (1985)
hydrotalcite	–1043.08	Allada *et al.* (2005)	–1165.98	Allada *et al.* (2005)
aluminite	–1333.11	ideal model (this study)	–1486.01	ideal model (this study)

conditions for EMP analysis were 15 kV accelerating potential, 4 nA sample current, 1 μm beam diameter. Standards used were diopside (for Ca, Mg and Si), Fe_2O_3 (for Fe), orthoclase (for Al), ZnS (for Zn and S), vanadinite (for Cl), $MnTiO_3$ (for Mn), Co (for Co), Cu (for Cu). A counting time of 10 s was applied for all elements. Elemental C, H and N analysis was carried out on a Perkin Elmer Series II CHN Analyser 2400: calibration and quality control were performed on a routine basis by the analysis of standard N-phenylacetamide.

The thermogravimetric and differential scan calorimetric curves were registered between 30 and 900 °C (10 °C/mn gradient) by a Netzsch STA 409 PC Luxx instrument. Microbalance and temperature calibration were performed by the manufacturer and checked periodically by TG analysis of a known compound (pentahydrate copper sulphate). The infra-red spectrum was obtained on a KBr disk with a Biorad Excalibur series FT-IR (resolution 2 cm^{-1}).

Scanning-electron microscopy was performed with a SEM Zeiss Supra 55VP of the Paris University, equipped with an EDX "silicon drift" detector PGT Sahara. Accelerating voltage was 15 kV. A semi-quantitative calibration of the elemental X-ray maps was made by using the software Spirit of PGT© (with background subtraction and peak deconvolution). The PCA of the elemental maps was performed using Multispec© software.

Table Xb. Heat capacity (C_p) data used in phase-diagram calculations.

Phase	Formula	Considered components	Reference	C_P 273.15 (J K^{-1} mol^{-1})	C_P 280.00 (J K^{-1} mol^{-1})	C_P298.15 (J K^{-1} mol^{-1})	a	$b \times 10^5$	c	d
chalcocyanite	$CuSO_4$	$CuO+SO_2+0.5O_2$	Weast (1985)	96.52	97.55	100.02	0.10440	3.23967	–1248.3	0.00000
malachite	$CuCO_3 \cdot Cu(OH)_2$	$2CuO+CO_2+H_2O$	Weast (1985)	176.52	177.18	178.95	0.16517	9.26914	305.6	-0.29865
cupric ion	Cu^{2+}	-	Puigdomemech & Taxén (2000)	-	-	–23.80	–0.02380	-	-	-
aluminum ion	Al^{3+}	-	Holland & Powell (1998)	-	-	–142.70	–0.14270	-	-	-
gibbsite	$Al(OH)_3$	-	Robie *et al.* (1979)	84.59	86.62	91.70	0.03565	17.49867	–1763.9	0.40953
quartz	SiO_2	-	Robie *et al.* (1979)	41.01	41.82	43.81	0.11070	–0.51890		–1.12830
sulphate ion	SO_4^{2-}	-	Weast (1985)	-	-	–292.88	–0.29288	-	-	-
spertiniite	$Cu(OH)_2$		Chase (1998)	94.96	94.98	95.24	0.16295	0.66039	1822.9	–1.55730
aluminum sulphate	$Al_2(SO_4)_3$	-	Robie *et al.* (1979)	233.72	241.47	259.41	0.07440	23.19921	–15200.1	4.95288
hydrotalcite s.s.	$Mg_{0.74}Al_{0.26}(OH)_2(CO_3)_{0.13} \cdot 0.39H_2O$	-	Allada *et al.* (2005)	93.28	95.46	101.34	–0.40394	67.63348	–2876.4	5.80153
aluminite	$Al(OH)_2(SO_4)_{0.5}$	$2/3Al(OH)_3+$ $1/6Al_2(SO_4)_3$	Robie *et al.* (1979)	95.35	97.99	104.37	0.03617	15.53231	–3709.3	1.09850
chrysocolla	$CuSiO_3 \cdot 2H_2O$	$Cu(OH)_2+SiO_2+$ H_2O	Robie *et al.* (1979), Chase (1998), Weast (1985)	234.00	225.48	208.37	2.14979	–82.01914	49143.3	–38.84585
dioptase	$CuSiO_3 \cdot H_2O$	$Cu(OH)_2+SiO_2$	Robie *et al.* (1979), Chase (1998)	126.28	128.30	133.18	0.22577	1.09367	–1413.3	–1.38064
water (liquid)	H_2O	-	Robie *et al.* (1979)	107.72	97.18	75.19	1.92401	-83.11281	50556.7	–37.46520
hydrogen ion	H^+	-	Weast (1985)	0.00	0.00	0.00	0.00000	0.00000	0.0	0.00000
carbon dioxide	CO_2	-	Robie *et al.* (1979)	36.13	36.40	37.13	0.08744	–0.23962	702.6	–0.99277
silicic acid	H_4SiO_4	-	Johnson *et al.* (1992)	-	-	468.98	0.46898	-	-	-

If not available, C_P for complex phases was calculated by adding the heat capacity of simple components (oxides, hydroxides and elements). The references for the C_P data of these components is also reported in the table. The variables a, b, c and d were derived from the function $C_P = a + bT + cT^{-2} + dT^{-1/2}$.

References

Allada, R.K., Navrotsky, A., Berbeco, H.T., Casey, W.H. (2002): Thermochemistry and aqueous solubilities of hydrotalcite-like solids. *Science*, **296**, 721-723.

Allada, R.K., Peltier, E., Navrotsky, A., Casey, W.H., Johnson, C.A., Berbeco, H.T., Sparks, D.L. (2006): Calorimetric determination of the enthalpies of formation of hydrotalcite-like solids and their use in the geochemical modeling of metals in natural waters. *Clays Clay Minerals*, **54**, 409-417.

Allada, R.K., Navrotsky, A., Boerio-Goates, J. (2005): Thermochemistry of hydrotalcite-like phases in the MgO-Al_2O_3-CO_2-H_2O system: A determination of enthalpy, entropy, and free energy. *Am. Mineral.*, **90**, 329-335.

Allmann, R. (1968): The crystal structure of pyroaurite. *Acta Crystallogr. Sect. B-Struct. Sci.*, **24**, 972-977.

Allmann, R. & Lohse, H.H. (1966): Die Kristallstruktur des Sjögrenits und eines Umwandlungsproduktes des Koenenits. *N. Jahrb. Mineral. Mh.*, **6**, 161-181.

Babéan, J. & Ševc, J. (1973): Beitrag zur Frage über die Entstehung und die Stabilität von Kupfermineralen im System Cu^{2+} – HCO_3^- – CO_3^{2-} – H_2O. *Geol. Carpath.*, **24**, 169-175.

Bellotto, M., Rebours, B., Clause, O., Lynch, J., Bazin, D., Elkaïm, E. (1996): A reexamination of hydrotalcite crystal chemistry. *J. Phys. Chem.*, **100**, 8527-8534.

Bertrand de Lom, J.-P. (1844): Description minéralogique et géologique de la mine de manganèse de Saint-Marcel en Piémont, et de quelques faits de même genre de la vallée où gît cette mine. *Echo du Monde savant,* **11**, 487-495.

Besse, M. & Vaccari, L. (1903): Excursion botanico-minéralogique faite dans les vallées de Saint-Marcel et de Cogne (Val d'Aoste). *Bulletin de La Murithienne, Société valaisanne des Sciences naturelles*, **32**, 87-108 [90-91].

Bourrié, G., Trolard, F., Refait, P., Feder, F. (2004): A solid-solution model for Fe(II)-Fe(III)-Mg(II) green rusts and fougerite and estimation of their Gibbs free energies of formation. *Clay Clay Minerals.*, **52**, 382-394.

Bravo-Suárez, J.J., Páez-Mozo, E.A., Oyama, S.T. (2004): Models for the estimation of thermodynamic properties of layered double hydroxides: application to the study of their anion exchange characteristics. *Quim. Nova*, **27**, 574-581.

Brindley, G.W. & Kikkawa, S. (1979): A crystal-chemical study of Mg,Al and Ni,Al hydroxyl-perchlorates and hydroxyl-carbonates. *Am. Mineral.*, **64**, 836-843.

Capitani, C. de & Brown, T.H. (1987): The computation of chemical equilibrium in complex systems containing non-ideal solutions. *Geochim. Cosmochim. Acta*, **51**, 2639-2652.

Certini, G., Wilson, M.J., Hillier, S.J., Fraser, A.R., Delbos, E. (2006): Mineral weathering in trachydacitic-derived soils and saprolites involving formation of embryonic halloysite and gibbsite at Mt. Amiata, central Italy. *Geoderma*, **133**, 173-190.

Cesti, G. (1978): Il giacimento piritoso-cuprifero di Chuc-Servette presso St. Marcel (Aosta). *Revue valdôtaine d'Histoire naturelle*, **32**, 127-156.

Chase, M.W.Jr. (1998): NIST-JANAF Themochemical Tables, Fourth Edition. *J. Phys. Chem. Ref. Data*, **9**, 1-1951.

Cheah, S.F., Brown Jr., G.E., Parks, G.A. (2000): XAFS study of Cu model compounds and Cu^{2+} sorption products on amorphous SiO_2, γ-Al_2O_3, and anatase. *Am. Mineral.*, **85**, 118-132.

Church, A.H. (1866a): Preliminary notice of a new Cornish mineral. *The Chemical News and Journal of Physical Science*, **13**, 85.

— (1866b): A new hydrated cupric-aluminium sulphate. *The Journal of the Chemical Society of London*, **4**, 130-135.

Delesse, A. (1846): Sur quelques produits résultant de la décomposition des minerais de cuivre. *Annales des Mines,* **(s.4) 9**, 587-606.

Dinelli, E. & Tateo, F. (2001): Factors controlling heavy-metal dispersion in mining areas: the case of Vigonzano (northern Italy), a Fe-Cu sulfide deposit associated with ophiolitic rocks. *Environ. Geol.*, **40**, 1138-1150.

—,— (2002): Different types of fine-grained sediments associated with acid mine drainage in the Libiola Fe–Cu mine area (Ligurian Apennines, Italy). *Appl. Geochem.*, **17**, 1081-1092.

Dinelli, E., Morandi, N., Tateo, F. (1998): Fine-grained weathering products in waste disposal from two sulphide mines in the northern Apennines, Italy. *Clay Minerals*, **33**, 423-433.

Faure, G. (1998): Principles and applications of geochemistry. 2nd edition. Prentice-Hall, London, 600 p.

Frau, F., Rizzo, R., Sabelli, C. (1998): Creedite from Sardinia, Italy: the first European occurrence. *N. Jahrb. Mineral. Mh.*, **11**, 495-504.

Fyfe, W.S., Turner, F.J., Verhoogen, J. (1958): Metamorphic reactions and metamorphic facies. Geological Society of America, Boulder, Memoir **73**, 259 p.

Gade, B., Pöllmann, H., Heindl, A., Westermann, H. (2001): Long-term behaviour and mineralogical reactions in hazardous waste landfills: a comparison of observation and geochemical modelling. *Environ. Geol.*, **40**, 248-256.

Göske, V.J., Witzke, T., Pöllmann, H., Stöber, S. (1997): Neufunde von Sekundärmineralen in der Lagerstätte Calamita/Insel Elba. *Der Aufschluss*, **48**, 305-313.

Grice, J.D. & Gasparrini, E. (1981): Spertiniite, $Cu(OH)_2$, a new mineral from the Jeffrey mine, Quebec. *Can. Mineral.*, **19**, 337-340.

Helgeson, H.C., Delany, J.M., Nesbitt, H.W., Bird, D.K. (1978): Summary and critique of the thermodynamic properties of rock-forming minerals. *Am. J. Sci.*, **278A**, 229 p.

Hensen, B.J. (1971): Theoretical phase relations involving cordierite and garnet in the system MgO–FeO–Al_2O_3–SiO_2. *Contrib. Mineral. Petrol.*, **33**, 191-214.

Hensen, B.J. & Green, D.H. (1971): Experimental study of the stability of cordierite and garnet in pelitic compositions at high pressures and temperatures. *Contrib. Mineral. Petrol.*, **33**, 309-330.

Hintze, C. (1930): Gruppe überbasischer Hydroxyl, bzw. Chlor enthaltender Sulfate zwei- und dreiwertiger Metalle. *in* "Handbuch der Mineralogie", ed., C. Hintze, Walter de Gruyter & Co., Berlin and Leipzig, Vol. 1, 4534-4543.

Holland, T.J.B. & Powell, R. (1998): An internally consistent thermodynamic data set for phases of petrological interest. *J. metamorphic Geol.*, **16**, 309-343.

Johnson, C.A. & Glasser, F.P. (2003): Hydrotalcite-like minerals ($M_2Al(OH)_6(CO_3)_{0.5}.XH_2O$, where M = Mg, Zn, Co, Ni) in the environment: synthesis, characterization and thermodynamic stability. *Clays Clay Minerals*, **51**, 1-8.

Johnson, J.W., Oelkers, E.H., Helgeson, H.C. (1992): SUPCRT92, a software package for calculating the standard molal thermodynamic properties of minerals, gases, aqueous species as a functions of temperature and pressure. *Computers Geosci.*, **18**, 899-947.

Keller, E. (1980): Kalottenmodelle. *Chemie in unserer Zeit*, **14**, 56-60.

La Motte, Saint-Martin count de (1784-85): Sur la fontaine verte de Saint-Marcel, dans la vallée d'Aoste. *Mémoires de l'Académie royale des Sciences [de Turin]*, **2**, 1-12.

Langford, J.I. (1978): A rapid method for analysing the breadths of diffraction and spectral lines using the Voigt function. *J. Appl. Crystallogr.*, **11**, 10-14.

Latimer, K.M. (1951): Method of estimating the entropy of solid compounds. *J. Am. Chem. Soc.*, **73**, 1480-1482.

— (1952): The oxidation states of the elements and their potentials in aqueous solutions. Prentice-Hall, Englewood Cliffs, New Jersey, 392 p.

Livingstone, A. (1990): Copper-aluminium analogues of hydrohonessite and honessite, and woodwardite relationship. *Mineral. Mag.*, **54**, 649-653.

Louër, M., Grandjean, D., Weigel, D. (1973): Etude structurale des hydroxynitrates de nickel et de zinc. II. Structure cristalline du nitrate basique de zinc $(Zn(OH)_2)_2\ Zn(NO_3)_2$. *Acta Crystallogr.*, **29**, 1703-1706.

Martin, S., Godard, G., Rebay, G. (2004): Walking on a palaeo ocean floor. The subducted Tethys in the Western Alps. *Journal of the Virtual Explorer [electronic ed., ISSN 1441-8142]*, **16**, paper 2.

Meixner, H. (1940): Über Woodwardit aus Cornwall und von Klausen (hier fälschlich „Langit" genannt) in Südtirol. *Zentralblatt für Mineralogie Abteilung A*, 238-244.

Nicco, R. (1988): L'industrializzazione in Valle d'Aosta; studi e documenti. *Quaderni dell'Istituto Storico della Resistenza in Valle d'Aosta*, **2**, 130 p. + 26 pl. [part I].

Nickel, E.H. (1976): New data on woodwardite. *Mineral. Mag.*, **43**, 644-647.

Nickel, E.H. & Clarke, R.M. (1976): Carrboydite, a hydrated sulfate of nickel and aluminum: a new mineral from Western Australia. *Am. Mineral.*, **61**, 366-372.

Noussan, É. (1972): Les fontaines colorées. *Bulletin de la Société de la Flore Valdôtaine*, **26**, 32-35.

Pelloux, A. (1908): I minerali del Gruppo del Gran Paradiso. *Bollettino del Club Alpino Italiano*, **39**, 157-188.

Peltier, E., Allada, R., Navrotsky, A., Sparks, D.L. (2006): Nickel solubility and precipitation in soils: a thermodynamic study. *Clays Clay Minerals*, **54**, 153-164.

Perel'man, A.I. (1986): Geochemical barriers: theory and practical applications. *Appl. Geochem.*, **1**, 669-680.

Prosio, P. (1903): L'eau verte de Saint-Marcel. *Bulletin de la Société de la Flore Valdôtaine*, **2**, 76-78.

Puigdomenech, I. & Taxén, C. (2000): Thermodynamic data for copper. Implications for the corrosion of copper under repository conditions. Technical report TR-00-13, Svensk Kärnbränslehantering AB, Stockholm, 96 p.

Raade, G., Elliott, C.J., Din, V.K. (1985): New data on glaucocerinite. *Mineral. Mag.*, **49**, 583-590.

Reynolds, R.C.Jr. (1989): Diffraction by small and disordered crystals. *Rev. Mineral.*, **20**, 145-181.

Robie, R.A. & Hemingway, B.S. (1995): Thermodynamic properties of minerals and related substances at 298.15 K and 1 bar (10^5 Pascals) pressure and at higher temperatures. *U. S. Geol. Surv. Bull.*, **2131**, 1-461.

Robie., R.A., Hemingway, B.S., Fisher, J.R. (1979): Thermodynamic properties of minerals and related substances at 298.15 K and 1 bar (10^5 Pascals) pressure and at higher temperatures. *U. S. Geol. Surv. Bull.*, **1452**, 1-455.

Saussure, H.-B. de (1796): Mines de Saint-Marcel. *in* "Voyages dans les Alpes, précédés d'un essai sur l'histoire naturelle des environs de Genève", ed., L. Fauche-Borel, Neuchâtel, Vol. 4, 454-459.

Scaini, G. (1971): La slavikite della miniera di Servette a Saint Marcel (Aosta). *Natura*, **62**, 135.

Schubert, M., Wennrich, R., Weiß, H., Schreck, P., Zeller, T., Otto, H.H., Wolfram, H. (2005): Formation of heavy metal bearing phases at a spring affected by the weathering of ore processing residues. *Eur. J. Mineral.*, **17**, 119-128.

Stara, P., Rizzo, R., Sabelli, C., Ibba, A. (1999): I minerali di Funtana Raminosa (Gadoni, Sardegna Centrale). *Rivista Mineralogica Italiana*, **1**, 10-27.

Terrana, S. (2006): Caratterizzazione idrogeologica dell'area mineraria di Servette (Saint Marcel – Valle d'Aosta). Unpublished graduation thesis, Università dell'Insubria, 129 p.

Thompson, H.A., Parks, G.A., Brown, G.E. (1999): Dynamic interactions of dissolution, surface adsorption, and precipitation in an aging cobalt(II)-clay-water system. *Geochim. Cosmochim. Acta*, **63**, 1767-1779.

Treacy, M.M.J., Newsam, J.M., Deem, M. W. (1991): A General Recursion Method for Calculating Diffracted Intensities from Crystals Containing Planar Faults. *Proc. R. Soc. A-Math. Phys. Eng. Sci.*, **433,** 499–520.

Watanabe, H., Tazaki, K., Islam, A.B.M.R., Chaerun, S.K. (2003): Copper biomineralization with banded structure at Dogamaru mine, Shimane Prefecture, Japan. *in* "Water and Soil Environments: Microorganisms play an important role", ed., K. Tazaki, Kanazawa University Press, Kanazawa, 91-140.

Weast, R.C. (1985): CRC handbook of chemistry and physics. CRC Press, Boca Raton, Florida.

Weil, R., Siat, A., Fluck, P. (1975): Espèces minérales inédites ou rares des Vosges. *Sciences Géologiques, Bulletin* [Strasbourg], **28**, 261-282.

Witzke, T. (1999): Hydrowoodwardite, a new mineral of the hydrotalcite group from Königswalde near Annaberg, Saxony/Germany and other localities. *N. Jahrb. Mineral. Mh.*, **2**, 75-86.

Witzke, T. & Raade, G. (2000): Zincowoodwardite, $[Zn_{1-X}Al_X(OH)_2][(SO_4)_{X/2}(H_2O)_n]$, a new mineral of the hydrotalcite group. *N. Jahrb. Mineral. Mh.*, **10**, 455-465.

Yakhontova, L.K., Postnikova, V.P., Vlasova, Y.V., Sergeyeva, N.Y. (1981): New data on posnjakite, serpierite and woodwardite. *Doklady Earth Sciences*, **256**, 144-148.

Yamaoka, T., Abe, M., Tsuji, M. (1989): Synthesis of Cu–Al hydrotalcite like compound and its ion exchange property. *Mater. Res. Bull.*, **24**, 1183-1199.

Received 26 February 2006
Modified version received 3 March 2007
Accepted 25 October 2007